Heterogeneous spatiotemporal streamflow response to large-scale climate indexes in the Eastern Alps

Teresa Pérez-Ciria [1,2]*, David Labat [3], Gabriele Chiogna [1,4]

[1] Faculty of Civil, Geo and Environmental Engineering, Technical University of Munich, Arcistr. 21, 80333 Munich, Germany

[2] Department of Geography, Ludwig-Maximilians-Universität München (LMU), Munich, Germany

[3] Géosciences Environnement Toulouse (GET), Université de Toulouse, IRD, CNES, CNRS, UPS, Toulouse 31400, France

[4] Department of Geography, University of Innsbruck, Innrain 52f, 6020 Innsbruck, Austria;

* Correspondence: teperez.ciria@tum.de

Abstract: Analyzing temporal and spatial variability of river discharge and the impacts of large-scale climate oscillations on hydrological systems are of particular interest in Alpine catchments, which have been proved to be especially sensitive to climatic drivers. The impact of climate oscillation indexes may show a delayed response and therefore the correlation between climatic drivers and streamflow is challenging to be properly identified. For this purpose, wavelet transform (WT) is recognized as a suitable tool able to determine the crucial scales of variability. In this work, first we explore the periodicities and the coherence among several climatic indexes: North Atlantic Oscillation Index (NAO), Mediterranean Oscillation Index (MO), Greenland Blocking Index (GB), and Artic Oscillation Index (AO). This analysis shows the complementary information that different oscillation indexes provide and the need to consider their impacts on streamflow simultaneously. Previous work revealed a heterogeneous and complex response of the Inn river basin at long temporal scales, which could not be linked to analyzed anthropogenic impacts such as dams' construction and hydropower plants operation. Therefore, the trigger of changes in streamflow variability remained unclear. In this study, we elaborate a classification based on all considered indexes' coherence with fifty gauging stations of the Inn river catchment. We quantify similarity among stations with a focus on yearly and longer temporal scales. The results highlight the heterogeneous response of the streamflow towards changes in climatic indexes and give an

overview of the possible drivers of detected long-term alterations. NAO and GB extreme phases are connected with cold winters and hot summers. We observe that from the 1980s changes detected in the streamflow behavior at yearly and longer temporal scales are in line with emerging patterns of the climatic indexes, such as the shift from constant to intermittent periodicities of the MO index. AO coherence displays a higher complexity able to capture singular hydrologic behaviors (i.e., particular hydrological regime only detected for one gauging station, often connected to high altitude small basins). From the cluster analysis we can also derive how mean catchment elevation and geographical location can contribute to the explanation of the influence and teleconnection to the oscillation indexes, while glacierized area is not identified as a dominant characteristic. Thus, this research contributes to a better understanding of streamflow variability over the Eastern Alps, and the role of teleconnection patterns on this variability. These relationships can be also used to improve hydrological forecasting and water resources management in the Alpine region.

Keywords: Streamflow variability, wavelet analysis, climatic indexes, spatiotemporal patterns, teleconnections.

Highlights

- Wavelet coherence applied for climate oscillation indexes and streamflow analysis
- Investigated periodicities proof complementarity among NAO, MO, GB and AO indexes
- Heterogeneous response of Alpine catchments towards changes in climatic indexes
- New streamflow classification method based on all considered indexes coherence
- Hydrological changes in the 1980s are detected with the proposed methodology

1. Introduction

Exploring streamflow variability in space and time and identifying relevant periodicities and alterations, which might be associated with large-scale climate indexes, is relevant to achieve a better understanding of hydrological systems (Pasquini and Depetris, 2007). Analyzing long-term variability is particularly important to understand the hydrological behavior of a catchment and its evolution. River discharge in Alpine catchments is very sensitive to climatic drivers, though climate variability may affect specific temporal scales and streamflow time series could show a delayed response to alterations (Beniston, 2006; Bocchiola, 2014; Quadrelli et al., 2001; Wanders and Wada, 2015). Hence, the correlation between climatic drivers and streamflow is challenging to be properly identified (Blöschl et al., 2019; Pérez Ciria and Chiogna, 2020; Rottler et al., 2020). The topographic characteristics of Alpine catchments lead to a more complex response of river discharge to climate change than catchments characterized by low elevation gradients (Engel et al., 2019). Previous work revealed a heterogeneous streamflow behavior at long temporal scales in the Inn river basin (Pérez Ciria and Chiogna, 2020). However, at temporal scales larger than one year we could not link the observed streamflow variability to anthropogenic impacts investigated in the region, such as dams' construction and hydropower plants operation (Pérez Ciria et al., 2019). Therefore, the trigger of changes in streamflow variability remained unclear. We aim at detecting the cause of hydrological anomalies by looking at the lagged correlation of climate oscillations to river discharge time series at targeted temporal scales.

At the global scale, Labat (2010) connected long-term mean-monthly flow fluctuations with climate indexes, showing that the dominant climate fluctuations that impact Europe are the North Atlantic Oscillation (NAO) and Arctic Oscillation (AO). Increasingly positive phases of

NAO index since 1980 have triggered persistent periods of high pressure over the Alps and have led to an amplified impact on the pressure field (Beniston and Jungo, 2002). In fact, snow cover throughout the European Alps has been decreasing during the 20th century, but especially since the 1980s (Matiu et al., 2021; Stewart, 2009). Glacier retreat has an impact on streamflow at long temporal scales, although basins might show a delayed response (Stahl et al., 2008). Moreover, there is evidence that the AO has a wide-ranging effect over the Northern Hemisphere and it is strongly coupled to surface air temperature fluctuations over the Eurasian continent (Kerr, 1999; Thompson and Wallace, 1998; Thompson and Wallace, 2000). Greenland Blocking (GB) episodes are connected to sea-ice losses, which have a global impact (van den Broeke et al., 2016). The assessment of these events' periodicities has become therefore relevant, since they are sporadic and exhibit a large natural variability (Michel et al., 2021; Woollings et al., 2018). Recently, related driving mechanisms (e.g.: increased anti-cyclonic conditions over Greenland, deep solar minimum) have been identified as triggers for NAO, AO and GB variability (Hanna et al., 2015). Furthermore, extensive research has been conducted to evaluate the influence of the MO index over southern Europe and vicinity areas (Cenk and Turgay, 2019; Dünkeloh and Jacobeit, 2003; Feidas et al., 2007; Törnros, 2013), where the main focus has been temperature and precipitation. Yearly correlation was found between MO and wet days in the Northeast of Italy (Brunetti et al., 2002) and annual precipitation of Mediterranean basins (Redolat et al., 2019). Additionally, the Mediterranean Oscillation (MO) has shown to be a relevant pattern in the North of Italy and Eastern Austria (Soja et al., 2013; Tsimplis and Shaw, 2008). From several studies we can infer that anomalies in the MO index will influence the alpine region (Corella et al., 2016; Criado-Aldeanueva and Soto-Navarro, 2013). However, in comparison with other large-scale indexes (e.g.: NAO index), little effort has been done to link anomalies and periodicities with streamflow in the

97 Alps. Additional indexes, such as the Atlantic Multidecadal Oscillation or El Niño-Southern
98 Oscillation did not display however clear results in the Central Alps (Fraedrich, 1994; Ranzi
99 et al., 2021) and are defined as having a weak impact on Alpine climate (Efthymiadis et al.,
100 2007).

101 Our analysis tests therefore the hypothesis that the impacts of climatic indices are propagated
102 to the river discharge variability at yearly and longer temporal scales. Among the oscillation
103 indexes affecting the Alpine region climate, we consider in this study the North Atlantic
104 Oscillation (NAO), the Mediterranean Oscillation (MO), Greenland Blocking (GB), and the
105 Arctic Oscillation (AO). This choice is motivated by previous studies that were able to
106 correlate these indexes with hydroclimatic alterations in the Alps or surrounding regions
107 (Casty et al., 2005; Lehr et al., 2012; Marzeion and Nesje, 2012) and underlined the necessity
108 for further research (Bartolini et al., 2009; Hanna et al., 2016; Marzeion and Nesje, 2012;
109 Scherrer et al., 2004; Soja et al., 2013; Steirou et al., 2017).

110 To determine and investigate the crucial scales of variability we apply wavelet transform (WT)
111 techniques. Wavelet analysis has shown to be a very promising tool to analyze non-stationary
112 hydro-climatic time series (Marcolini et al., 2017; Sang et al., 2018; Yeditha et al., 2021; Zolezzi
113 et al., 2009). In the past decades, it has found application in a wide range of climatological
114 studies based on oscillation indexes (Das et al., 2020; Fu et al., 2012; He et al., 2021; Jevrejeva
115 et al., 2003; Massei et al., 2010; Ranzi et al., 2021) and has been applied to investigate
116 streamflow variability in selected rivers worldwide (Agarwal et al., 2016; Labat, 2008; Labat,
117 2010; Labat et al., 2004; Massei et al., 2011; Nalley et al., 2012; Nalley et al., 2016; Nalley et al.,
118 2019; Pérez Ciria et al., 2019; Rossi et al., 2009). Our work introduces an original wavelet
119 transform approach to analyze the linkages between streamflow and the teleconnection

120 patterns variability. This technique allows us to identify common patterns between discharge
121 and climatic indexes, to investigate the impact of the climatic indexes on the gauging stations
122 and their complex and heterogeneous responses at multiple temporal scales. Furthermore, we
123 are able to identify the most relevant indexes for each region and the specific temporal periods
124 in which the impact is relevant.

125 Due to the singular hydrological and climatic conditions of the Alps (Bartolini et al., 2009;
126 Schaefli et al., 2007) a specific study targeting the heterogeneous correlation of climatic
127 indexes with river discharge is crucial. Our study aims at filling this research gap for the
128 Eastern Alps, trying to identify possible triggers of streamflow alteration at long-term
129 temporal scales. The innovative contribution of this work lies in i) the development of a
130 streamflow classification procedure for long temporal scales based on coherence values with
131 individual climatic indexes ii) the possibility to better understand heterogeneous relationships
132 at specific long temporal scales for individual indexes and all climatic indexes simultaneously,
133 and iii) the attribution or link of previously detected heterogeneities in streamflow variability
134 and the detection of stations with singular behavior (i.e., particular hydrological regime only
135 detected for one gauging station, often connected to high altitude small basins). Consistent
136 coherence patterns help us understand the sensitivity of particular regions within the Eastern
137 Alps to large-scale climate related impacts.

138 **2. Study area and data**

139 **2.1. The Inn River basin and its importance for climatic studies**

140 The study domain consists of the middle and upper part of the Inn river basin (Fig. 1a),
141 selected due to its topographic complexity, data availability (including a wide range of
142 catchment size and catchment mean elevation), and relevance of the Eastern Alps in Europe.

Moreover, the temporal variability of streamflow time series in the catchment was already investigated by Perez Ciria et al. (2019) and Perez Ciria and Chiogna (2020). The former work allows us to exclude as cause of detected changes in variability the effect of dams and hydropower plants construction and operation. While Perez Ciria and Chiogna (2020) offers us a term of comparison for the clustering analysis performed in this study. The region has a typically hydrological alpine regime, which implies humid and warm summers and autumns, snow and glacier-melt in spring and relatively dry winters (Korck et al., 2012). The mean annual air temperature in this area has a large variability, ranging from 2.8 °C in upper Inn catchment (above 1800 m a.s.l.) to 7.9 ºC in Wasserburg (period 1961 to 1990) (Auer et al., 2001), where the last gauging station considered in our study is located. The mean annual precipitation is 1200 mm (period 1990 to 2011) (Malagó et al., 2017; Ntegeka et al., 2013).

In this study, we consider daily streamflow time series (Q) from 50 gauging stations located along the Inn River basin and its tributaries (Table 1, Fig. 1a). The datasets and metadata used for this study were provided by the Swiss Bundesamt für Umwelt (Abteilung Hydrologie) (http://www.bafu.admin.ch), the Austrian Bundesministerium für Nachhaltigkeit und Tourismus (http://ehyd.gv.at), the Bavarian Hydrological Service, Bavarian Environmental Agency (http://www.gkd.bayern.de), the Austrian Glacier Inventory (Buckel and Otto, 2018) and the Swiss Glacier Inventory (Linsbauer et al., 2021). The physiographic characteristics and key features of each watershed are tabulated in Table 1. In our study only gauging stations that have more than 40 years of complete consecutive records were selected, which is considered as a valid length for meaningful statistical results for long-term analyses (Kahya and Kalaycı, 2004; Partal, 2010). Fig. 1b shows the classification obtained from the analysis of streamflow dynamics at multiple temporal scales from which the present study emerged.

166 **Figure 1**

167

168 **Table 1**. Characteristics of the selected watersheds of the Inn catchment (gauging station id, gauging
169 station name, river name, latitude, longitude, catchment area, percentage of glacierized area, mean
170 elevation of the catchment, and analyzed period, which is constraint by the length of both streamflow
171 time series and selected climate oscillation indexes time series).

Id	Station Name	River Name	Latitude	Longitude	Catchment Area (km^2)	% glacierized area	Mean catchment elevation (m a.s.l.)	Analyzed period
1	Anger	Attel	48°01'26"	12°08'52"	249.60	0	535	1950-2013
2	Bad Aibling	Glonn	47°51'38"	12°00'38"	144.10	0	516	1948-2014
3	Berninabach - Pontresina	Ova da Bernina	46°29'11"	09°54'22"	107.00	16.76	2615	1954-2017
4	Bleyerbrücke	Kieferbach	47°36'50"	12°09'23"	116.40	0	1077	1950-2014
5	Brixlegg	Inn	47°25'59"	11°52'24"	8503.60	2.81	2010	1976-2015
6	Bruckhäusl	Brixentaler Ache	47°29'28"	12°06'16"	321.08	0	1331	1951-2015
7	Cinuos-Chel	Inn	46°38'08"	10°01'15"	733	0.05	2456	1974-2017
8	EKW-Valtorta	Pumped water	46°38'08"	10°01'15"	-	0	-	1974-2017
9	Erb - Leitzach	Leitzach	47°53'12"	11°49'45"	202.70	0	964	1948-2014
10	EW-Gmünd	Gerlosbach	47°12'42"	12°00'18"	140.54	1.92	1957	1976-2015
11	Feldolling	Mangfall	47°53'34"	11°51'09"	754	0	921	1948-2014
12	Galtür-Au	Trisanna	46°58'23"	10°11'56"	97.60	5.65	2361	1966-2015
13	Hart im Zillertal	Ziller	47°20'49"	11°51'46"	1094.19	2.89	1921	1966-2015
14	Hörbrunn	Kelchsauer Ache	47°25'15"	12°08'25"	134.21	0	1548	1971-2015
15	Huben	Ötztaler Ache	47°02'37"	10°58'24"	516.91	13.67	2614	1976-2015
16	Innsbruck	Inn	47°16'34"	11°23'49"	5771.60	3.25	2138	1951-2015
17	Innsbruck-Reichenau	Sill	47°16'24"	11°24'43"	853.11	2.28	1899	1951-2015

18	Jenbach	Inn	47°23'22"	11°47'23"	7230.70	2.87	2045	1971-2015
19	Kajetansbrücke	Inn	46°57'09"	10°30'43"	2148	2.30	2319	1951-2015
20	Kirchbichl	Inn	47°31'24"	12°05'38"	9310	2.56	1940	1951-2015
21	Klaushof (Brücke)	Ziller	47°09'27"	11°56'34"	135.28	2.92	2250	1951-2015
22	Landeck-Bruggen	Sanna	47°08'39"	10°33'49"	727	1.17	2124	1971-2015
23	Magerbach	Inn	47°15'34"	10°52'30"	5118.80	3.59	2212	1951-2015
24	Mariathal	Brandenberger Ache	47°27'19"	11°51'56"	271.88	0	1239	1976-2015
25	Martina	Inn	46°53'09"	10°27'56"	1941	2.53	2343	1948-2017
26	Mayrhofen	Ziller	47°10'09"	11°51'37"	611.07	4.72	2128	1966-2015
27	Oberaudorf	Inn	47°38'39"	12°11'47"	9713.20	2.46	1903	1948-2015
28	Persal	Tuxbach	47°08'59"	11°48'49"	129.26	3.03	2045	1961-2015
29	Prutz	Inn	47°04'38"	10°39'41"	2461.50	2.02	2283	1951-2015
30	Puig	Sill	47°06'49"	11°27'10"	342.12	0.57	1910	1951-2015
31	Punt dal gall	Spöl	46°37'45"	10°11'41"	295	0	2389	1974-2017
32	Rohr	Gerlosbach	47°14'15"	11°53'53"	197.40	1.37	1870	1966-2015
33	Rosenheim	Inn	47°51'15"	12°08'37"	10153.50	2.35	1859	1971-2015
34	Rosenheim tributary	Mangfall	47°50'41"	12°07'31"	1094.60	0	829	1966-2014
35	Sausteinaste	Zemmbach	47°07'25"	11°48'38"	225.57	8.57	2280	1956-2015
36	Schalklhof	Schalklbach	46°56'17"	10°29'24"	107.80	0.11	2276	1971-2014
37	Schmerold	Mangfall	47°46'24"	11°46'06"	222.70	0	1068	1948-2014
38	See im Paznauntal	Trisanna	47°05'13"	10°28'09"	385.40	1.69	2235	1971-2015
39	St. Anton am Arlberg-Moos	Rosanna	47°07'20"	10°15'23"	130.60	1.11	2250	1966-2015
40	St. Jodok am Brenner	Valser Bach	47°03'47"	11°30'00"	109.20	1.08	2019	1951-2015
41	St. Leonhard im Pitztal	Pitze	47°04'13"	10°50'38"	165.31	14.35	2560	1961-2015
42	St. Moritzbad	Inn	46°29'05"	09°50'03"	155	3.72	2399	1948-2017
43	Steinach am Brenner	Gschnitzbach	47°05'36"	11°27'57"	111.58	0.67	1952	1951-2015

44	Strengen	Rosanna	47°07'29"	10°27'57"	271.30	0.71	2085	1966-2015
45	Tarasp	Inn	46°47'21"	10°16'43"	1581	3.08	2384	1957-2017
46	Tumpen	Ötztaler Ache	47°09'48"	10°54'39"	784.27	10.29	2481	1951-2015
47	Valley	Mangfall	47°53'43"	11°47'00"	381.70	0	955	1950-2014
48	Wasserburg	Inn	48°03'33"	12°14'03"	11960.40	2	1681	1965-2014
49	Weichselbaum	Murn	47°58'48"	12°12'44"	162.70	0	503	1971-2015
50	Zell am Ziller-Zellbergeben	Ziller	47°14'07"	11°52'50"	696.26	4.15	2055	1951-2015

2.2. Climate index data

In this study we will focus on the impact of NAO, MO, GB and AO indexes.

The North Atlantic Oscillation (NAO) is a prominent pattern of climate variability defined as the difference of atmospheric pressure at sea level between two regions, one typically located near Iceland (sub-polar low) and the other over the Azores (subtropical high). The high latitudes of the North Atlantic Ocean near Greenland and Iceland generally experience lower air pressure than surrounding regions. Whereas in the south, air pressure over the central North Atlantic Ocean is generally higher than surrounding regions (Dahlman, 2009). The NAO index data was taken from the website of the NOAA's Climate Prediction Center's (CPC) (http://www.cpc.ncep.noaa.gov).

The Mediterranean Oscillation (MO) Index represents the behavior of the atmosphere in the area between the western and eastern Mediterranean Sea. Changes in temperature, precipitation, streamflow and other parameters are highly related to the MO. There are different versions of the MO: i) MO.1 (Conte et al., 1989; Palutikof et al., 1996) is defined as the normalized pressure difference between Algiers (36.4°N, 3.1°E) and Cairo (30.1°N, 31.4°E); ii) the second version of the index, MO.2 (Palutikof, 2003), can be calculated from the

difference on sea level pressure between Gibraltar's Northern Frontier (36.1°N, 5.3°W) and Lod Airport in Israel (32.0°N, 34.5°E). The MO data, both MO.1 and MO.2 time series data, was taken from the website of the Climatic Research Unit of the University of East Anglia in Norwich, UK (http://www.cru.uea.ac.uk). The analysis was conducted for both versions. However, due to the similar obtained results we only show findings linked to the MO.2, which displayed strongest impact on the study area.

The Greenland Blocking (GB) is the mean 500-hPa geopotential height over the Greenland region, from 20° to 80°W and 60° to 80°N. GB occurs when there is a breaking of synoptic-scale Rossby waves resulting in a quasi-stationary high pressure system that blocks circulation (Barrett et al., 2020), typically resulting in a large-scale reversal of the meridional geopotential height gradient (Pelly and Hoskins, 2003) and causing cold temperatures and snow over Europe. The daily index is available in https://www.esrl.noaa.gov/.

The Arctic Oscillation (AO) is defined as the first Empirical Orthogonal Function (EOF) of the mean sea level pressure field in the Northern Hemisphere (Ambaum et al., 2001). It is an annular-like mode in the northern extratropical circulation which has an equivalent barotropic structure from the surface to the lower stratosphere (Thompson and Wallace, 1998). This mode exists in both hemispheres (Gong and Wang, 1999; Thompson and Wallace, 2000) and it has two same-signed centers of action over the Pacific and Atlantic Ocean. Fluctuations in the AO create a see-saw pattern in which atmospheric pressure at northern polar and middle latitudes alternates between positive and negative phase (Gong et al., 2001). The AO data was taken from the website of the NOAAs Climate Prediction Center's (CPC) (http://www.cpc.noaa.gov).

3. Methods

The Continuous Wavelet Transform (CWT) and Wavelet Coherence (WTC) among the indexes was conducted to have a complete understanding of the periodicities and patterns that govern their behavior at long temporal scales. The WTC was computed between streamflow and climate indexes time series and used to elaborate the classification based on individual climate indexes and all indexes.

3.1. Continuous Wavelet Transform (CWT)

The CWT is used to determine if periodicities are present in a signal and to detect at which scales and time period they are dominant. The CWT of a discrete sequence x_n, with constant time spacing δt, is defined as the convolution of x_n with a scaled and translated version of $\psi_0(\eta)$:

$$W_n(s) = \sum_{n'=0}^{N-1} x_{n'} \psi^* \left[\frac{(n'-n)\delta t}{s} \right] \quad (1)$$

where the (*) designates the complex conjugate, n is the localized time index, n' is the time variable, s is the wavelet scale and N is the number of points in the time series. To resolve localized signals, Morlet wavelet is chosen as the mother wavelet, since it is good for feature extraction and it provides a good compromise between the time and frequency resolution (Grinsted et al., 2004). Only periodicity different from red noise within 95% confidence intervals estimated by Monte Carlo simulations are taken into consideration and therefore the significance level of each scale is evaluated using the values outside the cone of influence (COI), where the edge effects could become significant and may affect the results reliability (Torrence and Compo, 1998).

3.2. Wavelet Coherence (WTC)

The wavelet coherence between two time series can be interpreted as a localized squared correlation coefficient in time-frequency space (Torrence and Webster, 1999). Coherence varies between 0 (uncorrelated) to 1 (fully correlated) and it is defined as follows (Torrence and Webster, 1999):

$$R_n^2(s) = \frac{|S[s^{-1}W_n^{XY}(s)]|^2}{S[s^{-1}|W_n^X(s)|^2]\, S\,[s^{-1}|W_n^Y(s)|^2]} \quad (2)$$

where S is a smoothing operator, given by $S(W) = S_{scale}\{S_{time}[W_n(s)]\}$, while S_{scale} denotes smoothing with respect to scales s and S_{time} smoothing in time.

Cause-effect relationships can be assessed by evaluating the wavelet phase angle that ranges between 0 and 360°. The relative phase relationship between two variables is represented by arrows. Horizontal arrows pointing to the right represent 0° phase difference (overlapping sine waves). Horizontal arrows pointing to the left reveal a 180° phase difference, which indicates counter-phase behavior. Regions of high coherence with a consistent phase relationship, which might change progressively, suggest causality between the time series (Grinsted et al., 2004; Schuler et al., 2021).

3.3. Clustering process and streamflow response assessment

From the coherence between streamflow time series and climatic oscillation indexes, we cluster the gauging stations behavior for each individual climatic index and elaborate the corresponding maps.

To quantitatively evaluate if two gauging stations (e.g.: gauging stations A and B) present the same patterns with an individual index, we compare coherence results by computing a metric based on the mean absolute difference (MD) for each time-frequency output.

$$MD_{index,A,B} = \frac{\sum_{x=1}^{n}\sum_{y=1}^{m}\left|R_{A\,x,y} - R_{B\,x,y}\right|}{n\ x\ m} \quad (3)$$

253 R (ranging from 0 to 1) represents the coherence value for a specific time (x) and frequency
254 (y), m is the largest frequency considered and n is the length of the shortest between the two
255 considered time series. We consider that two stations belong to the same cluster if MD is lower
256 than 10%. This threshold could be dependent on the dataset. In this case, a 10% threshold
257 empirically allows a coherent discrepancy between the different gauging stations. Thus, if the
258 wavelet coherence results of a gauging station (e.g.: gauging station C) with a specific climatic
259 index (e.g.: Arctic Oscillation Index) do not present MD lower that 10% with any other
260 analyzed gauging stations, then the abovementioned gauging station (i.e.: gauging station C)
261 is considered "not classified" for this specific index.
262 The classifications are finally merged to consider the behavior of each specific gauging station
263 with all indexes. The merging procedure consists in overlapping the classification results
264 obtained for individual indexes. Each specific combination (e.g., gauging stations classified
265 as NAO1, MO1, GB1 and AO1) will be designated as a specific cluster (e.g., cluster A) of the
266 classification based on all indexes. Only stations that are considered "not classified" for all
267 indexes, are denominated "not classified" in the classification based on all indexes. When this
268 is not the case, and the gauging station belongs to a specific class for at least one of the assessed
269 indexes, then we classify it as "singular behavior".
270 We evaluate the similarity of our classification based on all indexes with the classification
271 based on streamflow dynamics presented in Pérez Ciria and Chiogna (2020), which was an
272 inter-comparison of streamflow time series at multiple temporal scales. It showed the
273 distribution of stations characterized by snow dynamics, rain-fed basins and how contrasting
274 streamflow patterns emerged at large temporal scales, especially from the 1980s. The

similarity is therefore assessed by computing the Adjusted Rand Index (ARI). Given a set of n elements, and two classifications of these elements, namely $X = \{X_1, X_2, \ldots, X_i\}$ and $Y = \{Y_1, Y_2, \ldots, Y_j\}$, the overlap between X and Y can be computed as follows:

$$ARI = \frac{\sum_{ij}\binom{n_{ij}}{2} - \left[\sum_i \binom{a_i}{2}\sum_j \binom{b_j}{2}\right]/\binom{n}{2}}{\frac{1}{2}\left[\sum_i \binom{a_i}{2} + \sum_j \binom{b_j}{2}\right] - \left[\sum_i \binom{a_i}{2}\sum_j \binom{b_j}{2}\right]/\binom{n}{2}} \quad (4)$$

n_{ij} denotes the number of objects in common between the clusters. a_i and b_j denote the number of objects per cluster X_i and Y_j, respectively.

From this comparison we investigate the level of agreement of our results. We are able to attribute discrepancies, if present, to specific gauging stations by means of an approach based on evidence of "total agreement", "partial agreement", or "strong disagreement":

- "Total agreement" implies that there is a complete overlap of the stations
- "Partial agreement (larger streamflow variability)". This implies that there are discrepancies in hydrological behavior that cannot be linked to the coherence analysis with the selected climate indexes.
- "Partial agreement (unique hydrological behavior)", indicates that these gauging stations belong to a specific cluster when analyzing climate indexes impacts, but showed a unique hydrological regime.
- "Partial agreement (larger climatic variability)", in this case represents gauging stations that show a more heterogenous response while analyzing their coherence with climate indexes, but belonged to the same cluster for streamflow behavior.
- "Strong disagreement" represents stations that were classified in a completely different cluster (no overlap).

295 A step-wise description of the clustering process and streamflow response assessment is
296 provided in Fig. 2.

297 **Figure 2**

298 **4. Results**

299 **4.1. Wavelet analysis of climate oscillation indexes**

300 CWT results of the selected climate oscillation indexes are shown in Fig. 3. The ordered axis
301 presents the time in years and the analyzed periods are represented in the abscissa axis. The
302 normalized time series used for the wavelet analysis are included in Fig. S1. As we observe
303 in Fig. 3a, NAO index does not show a clear intra-annual variability and therefore we do not
304 observe a constant statistically significant pattern at the yearly scale. We detected however
305 that high-power values are present in 1990 and from 2010. The multi-year scales display
306 higher power than the yearly scale in general. We can observe high wavelet power bands
307 associated to 2-4 years and also a continuous high-power band at 8 years-scale. In Fig. 3b the
308 CWT of the Mediterranean Oscillation Index (MO) presents high power at the yearly scale,
309 which implies a very strong intra-annual variability. We observe this strong periodicity from
310 the beginning of the analyzed period. Nevertheless, this pattern seems to fade in 1980 and it
311 becomes intermittent. Thus, gauging stations that present high coherence with MO during
312 the whole analyzed period are actually characterized by an intermittent loss of the yearly
313 periodicity from the 1980s. Additionally, we observe high power bands during the analyzed
314 period at 5 years and 10 years scales. For the Greenland Blocking CWT (Fig. 3c) the strongest
315 yearly pattern is detected. No significant high-power patterns are detected however at multi-
316 year scales. From this, we are able to anticipate that the identified clusters will be mainly
317 driven by the correlation found at the yearly scale. The Arctic Oscillation Index CWT (Fig. 3d)

318 does not show a clear intra-annual variability. Similar to NAO, the multi-year scales display
319 high power. We can observe a high wavelet power bands associated to 2-4 years and 8 years-
320 scale.
321 **Figure 3**
322 WTC among considered climate indexes at long temporal scales is shown in Fig.4. We can
323 observe high coherence values in phase: at yearly scale between MO and GB (Fig. 4d), and
324 with intermittent presence at 2-4 years scale between NAO and AO (Fig.4e). High coherence
325 values in counterphase are also present: at 2-4 years scale between NAO and GB (Fig. 4c), and
326 at multiannual scales between AO and GB (Fig. 4f). Additionally, we observe low coherence
327 values or only sporadic high coherence spots: from yearly to 8 years scale between NAO and
328 MO (Fig. 4a) and between MO and AO (Fig. 4b); at yearly scale between NAO and GB (Fig.
329 4c) and also at yearly scale between AO and GB (Fig. 4f); at 2-8 years scale between MO and
330 GB (Fig. 4d); at 4-8 years scale between NAO and AO (Fig. 4e). Even if the high correlation of
331 some indexes, such as NAO and AO (Ambaum et al., 2001; Hamouda et al., 2021), is
332 confirmed by the coherence analysis, the coherence among indexes displays a variety of
333 patterns depending on the targeted temporal scale. This implies that each selected oscillation
334 index carries different information that might contribute to understand patterns of
335 hydrometeorological variables.
336 **Figure 4**
337
338 **4.2. Wavelet coherence between streamflow and climate oscillation indexes**
339 Fig. 5 shows an illustrative example of the coherence outcome considering three different
340 gauging stations and the four selected climatic indexes. Fig. S2 contains the entire analysis (50
341 coherence plots per climatic index). From the comparison of Fig. 5a (wavelet coherence

342 between NAO index and Innsbruck streamflow time series) with Fig. 5b (wavelet coherence
343 between NAO index and Kirchbichl streamflow time series), we can observe that the same
344 patterns are present during the analyzed time span. Focusing on the yearly scale, intermittent
345 patterns in phase (arrows pointing right) are present till 1980. From this year intermittent
346 patterns characterized by high coherence values are observed, but presenting a counter-phase
347 behavior (arrows pointing left). At longer temporal scales only sporadic high coherence spots
348 associated to 2 years scale are detected in 1960 and 1980. These two gauging stations present
349 resembling coherence patterns with NAO index with a mean absolute difference (MD) of
350 0.0499 (Table 2). They belong therefore to the same class, in this case NAO1-2 (see Fig.6 and
351 Table 3). Analogously, when comparing Fig. 5 left panel (Innsbruck streamflow time series)
352 with Fig. 5 middle panel (Kirchbichl streamflow time series) we observe that the coherence
353 results present identical patterns along the analyzed time span with MD lower than 10%
354 (Table 2). In particular, for the WTC with MO, both plots (Fig. 5d and Fig. 5e) present high
355 coherence at the yearly scale and a pattern associated to the 4-8 years scale emerges in the
356 1980s. The WTC with GB shows for Fig. 5g and Fig. 5h a very strong coherence at yearly scale,
357 which is due to the intra-annual variability characteristic of snow dominated regions. The
358 WTC with the AO index shows in both Fig. 5j and Fig. 5k that a high coherence pattern
359 associated to the 4-6 years scale stops in 1980. Thus, for the classification based on all indexes,
360 we conclude that Innsbruck and Kirchbichl belong both to class D (see Table 3 and Fig. 7).
361 The comparison of Fig. 5 left panel (Innsbruck streamflow time series) and Fig.5 right panel
362 (Anger streamflow time series) illustrates contrasting results with MD values larger than 20%
363 (Table 2), exceeding the established threshold of 10%. Fig. 5f does not show a constant yearly
364 periodicity as it is observed in Fig. 5d (and Fig. 5e), but only intermittent high coherence
365 patterns. Additionally, the in-phase pattern observed at the 4-8 years scale from the 1980s in

366 Fig. 5d (and Fig. 5e) is not present in Fig. 5f. Thus, the gauging station located in Anger
367 belongs to a different class (class K based on all indexes) (see Table 3 and Fig. 7).

368 **Figure 5**

369

370 **Table 2**. Mean absolute difference (MD) among coherence results shown in Fig. 5.

Climate oscillation index	Innsbruck - Kirchbichl	Innsbruck - Anger	Anger - Kirchbichl
NAO	0.0499	0.2102	0.1987
MO	0.0522	0.2482	0.2367
GB	0.0518	0.2805	0.2648
AO	0.0535	0.2065	0.1861

371

372 ### 4.3. Classification results

373 The classifications based on individual indexes are presented in Fig. 6 and Table 3. Fig. 6
374 contains four maps, each of them with the geographical distribution of the clusters detected
375 for the individual climatic index. In Fig. 6 stations that displayed the same coherence results
376 at yearly scale with the indicated index are represented with the same color. Additionally, if
377 those stations presented any different behavior at longer temporal scales, the different clusters
378 maintain the same color but are represented by different symbols. The sub-class at multi-
379 annual scales is represented by the sub-class number; while grey crosses represent "not
380 classified" stations (mean absolute difference values higher than 10% with all analyzed
381 stations).

382 **Figure 6**

383 We merge the obtained clusters for each individual index to obtain the classification based on
384 all indexes (Fig. 7a). The overlay of clusters highlights the heterogeneous response of the
385 catchments and the difficulty to attribute a unique trigger to a particular alteration. Fig. 7b

displays the level of agreement of the classification based on all indexes with the classification based on streamflow dynamics at multiple temporal scales (Fig.1b).

Table 4 displays the matching matrix between both classifications needed for the Adjusted Rand Index (ARI) computation. The 50 gauging stations are in this work the set of n elements mentioned in Eq. 4 description. Each element of Table 4 (n_{ij}) denotes the number of objects in common between the clusters (i.e., number of gauging stations in common). The values of the last column and the last row (a_i and b_j) denote the total number of gauging stations per cluster (e.g., 5 gauging stations belong to cluster A). By computing ARI (Eq. 4) we can therefore assess the overlap between two classifications of these elements, namely "classification based on all indexes" and "classification based on streamflow dynamics" presented in Pérez Ciria and Chiogna (2020).

ARI for both classifications is 0.4, which shows a relatively high level of agreement considering the heterogeneity of the stations with singular behavior (classification based on all indexes) and the not classified stations (classification based on streamflow dynamics).

From the comparison of the two different classification approaches we can highlight there is a total agreement of the cluster for 58% of the stations. Moreover, consistent results are found for 90% of the stations. This includes gauging stations that displayed total agreement and partial agreement with a more homogeneous cluster distribution than the classification based on streamflow dynamics.

Only 2% of the analyzed gauging stations show disagreement in Fig.7b. However, 40% of the gauging stations show partial agreement. From the partial agreement we observe that 24% of the gauging stations were classified in a different cluster when considering streamflow variability, but displayed common patterns with a larger group of gauging stations in the

409 classification based on all indexes. 8 % of the gauging stations belong to a specific class based
410 on all indexes, but were identified as not classified based on streamflow dynamics. These two
411 groups highlight the presence of additional triggers as cause of the detected streamflow
412 variability (e.g.: geomorphological characteristics, surface-groundwater interaction, water
413 uses). On the other hand, 8% of the analyzed gauging stations are classified in an additional
414 cluster for the classification based on all indexes. This discrepancy is originated by the
415 classification performed while analyzing the coherence at long temporal scales with the AO
416 index. Thus, Fig. 7 points out regions of interest that deserve further study. For example,
417 stations that belong to Class B and C, which showed homogeneous behavior based on
418 streamflow dynamics but larger climatic variability or gauging stations with singular
419 behavior.
420 In the following sections we provide an in-depth assessment of the clusters detected based on
421 coherence results with each individual climatic index and we explore the reasons behind
422 changes in streamflow periodicities. Localized particular behaviors, such as isolated
423 discontinuities at yearly scale, have been verified with the information gathered in a previous
424 study. For detailed information regarding anthropogenic impacts in the case study region,
425 please see Pérez Ciria et al. (2019).

426 **Table 3.** Classification obtained from the WTC analysis of 50 gauging stations along the Inn River and
427 its tributaries according to their response to climate oscillation indexes (NAO, MO, GB, and AO
428 indexes). The gauging stations are clustered based on the observed patterns at i) the yearly scale
429 (represented by the first number that follows the climate index acronym), and ii) longer temporal
430 scales, which are only represented by a second number indicating a sub-class for gauging stations that
431 showing the same yearly patterns display a different behavior when analyzing longer temporal scales.
432 Gauging stations that presented a peculiar behavior are categorized as "not classified" (NC). The last

two columns include a summary of the class identified for each climate index and the class based on all indexes. Basins which were not classified for a specific index are categorized as basins with "singular behavior".

NAO	MO	GB	AO	Gauging stations		Classification based on all indexes	
NAO1-1	MO1-1	GB1-1	AO1-1	Galtür-Au Landeck-Bruggen See im Paznauntal	St. Anton am Arlberg-Moos Strengen	NAO1-1 MO1-1 GB1-1 AO1-1	**A**
NAO1-2		GB1-2	AO1-2	Berninabach - Pontresina Cinuos -Chel	St. Moritzbad Tarasp	NAO1-2 MO1-1 GB1-2 AO1-2	**B**
			AO1-3	Kajetansbrücke Magerbach Martina	Prutz St. Leonhard im Pitztal	NAO1-2 MO1-1 GB1-2 AO1-3	**C**
			AO1-4	Innsbruck Jenbach Brixlegg Kirchbichl-Bichlwang Oberaudorf Rosenheim Wasserburg	Bruckhäusl Hart im Zillertal EW-Gmünd Mayrhofen Rohr Zell am Ziller-Zellbergeben	NAO1-2 MO1-1 GB1-2 AO1-4	**D**
			AO1-5	Huben Tumpen Innsbruck-Reichenau	Puig St. Jodok am Brenner	NAO1-2 MO1-1 GB1-2 AO1-5	**E**
	MO1-2			Persal		NAO1-2 MO1-2 GB1 AO1-5	**F**
NAO2-1	MO2	GB2	AO2-1	Bleyerbrücke Mariathal Schmerold		NAO2-1 MO2 GB2 AO2-1	**G**
	MO3	GB3	AO2-2	Valley		NAO2-1 MO3 GB3 AO2-2	**H**
NAO2-2				Erb - Leitzach Feldolling		NAO2-2 MO3 GB3 AO2-2	**I**
	MO2		AO3	Rosenheim tributary		NAO2-2 MO2 GB3 AO3	**J**
NAO3	MO4	GB4		Anger Bad Aibling Weichselbaum		NAO3 MO4 GB4 AO3	**K**
NAO1-1	MO1-1	GB1-1	Not classified (NC)	Schalklhof		Singular behavior	
		GB1-2		Punt dal gall			
NAO1-2				EKW-Valtorta Hörbrunn	Klaushof (Brücke) Steinach am Brenner		
	MO1-2			Sausteinaste			

Table 4. Matching matrix for the computation of the Adjusted Rand Index (ARI) (Eq. 4). Each element (n_{ij}) denotes the number of objects in common between the clusters (i.e., number of gauging

stations in common). The values of the last column and the last row (a_i and b_j) denote the total number of gauging stations per class. The sum of the objects in the last column indicates the set of classified elements, in this case 50 gauging stations (analogously for the last row).

Class based on all indexes	Class based on streamflow dynamics														Stations per class
	1	2	3	4	5	6	7	8	9	10	11	12	13	NC	
A	0	4	0	0	0	0	0	0	0	0	0	0	0	1	5
B	3	0	0	0	0	0	0	0	0	0	0	0	0	1	4
C	3	0	1	0	0	0	0	0	0	0	0	0	0	1	5
D	0	0	4	3	0	0	3	3	0	0	0	0	0	0	13
E	0	0	0	0	2	3	0	0	0	0	0	0	0	0	5
F	0	0	0	0	0	0	0	0	0	0	0	0	0	1	1
G	0	0	0	0	0	0	0	0	2	0	0	0	0	1	3
H	0	0	0	0	0	0	0	0	0	0	1	0	0	0	1
I	0	0	0	0	0	0	0	0	0	0	2	0	0	0	2
J	0	0	0	0	0	0	0	0	0	1	0	0	0	0	1
K	0	0	0	0	0	0	0	0	0	0	0	1	2	0	3
Singular behavior	0	0	0	0	0	0	0	0	0	0	0	0	0	7	7
Stations per class	6	4	5	3	2	3	3	3	2	1	3	1	2	12	Stations Total 50

5. Discussion

5.1. Classification based on individual indexes

5.1.1. NAO index

Firstly, focusing on the yearly scale, we determined an evident pattern that is present in all the analyzed stations that belong to cluster NAO1 (80% of the stations). The detected pattern consists of occasional yearly high coherence values in phase till 1980, followed by a shift to counter phase and more frequent high coherence values starting from the 1980s. NAO1 is characterized by nested catchments including all station located in the main Inn river, while NAO2 and NAO3 stations are located at tributaries of the Inn. NAO2 cluster displays medium to high coherence values from the 1980s but with a 90° phase shift. The coherence is particularly strong in the late 1980s and in 2000. The NAO3 cluster presents a different yearly

456 pattern, showing intermittent high coherence from 1965 till 1980 and a loss of coherence from
457 the 1980s with an isolated spot of high coherence in phase in 2000.

458 At longer temporal scales we observe in NAO1 high coherence in counter-phase around 1980
459 at the 2 years scale and a strong signal associated to 4-8 years scales starting from 2000. For
460 the stations within the Sanna River Basin (NAO1-1) intermittent high coherence values at the
461 2-4 years scale are spotted in the late 1980s (counter-phase), around 2000 (in phase) and from
462 2010 (counter-phase). NAO2 presents at 2-4 years scale statistically significant high coherence
463 from the late 1970s till 1990 (counter-phase). High coherence between NAO and this second
464 cluster returns at the 2-4 years scale from 2005. For NAO3 stations, which already presented
465 a strong difference in WTC behavior at the yearly scale, at multi-temporal scales we can
466 recognize medium to high coherence values within the 1980s, but with lower power, and
467 during a shorter period than the patterns observed for the cluster NAO2. Gauging stations
468 belonging to cluster NAO3 present therefore the weakest coherence signals with NAO and
469 are characterized by mean catchment elevations lower than 1000 m a.s.l. (Fig. S3). These
470 findings agree with previous studies (Beniston et al., 2018; Beniston and Jungo, 2002) that
471 reveal that at low elevations the NAO impact is rather weak or even absent in the Alpine
472 region, while higher elevation sites are sensitive to changes in NAO patterns.

473 During negative significant NAO index phases (e.g.: 1962, 1968), high coherence in phase at
474 the yearly scale is found with most of the stations within the Inn river basin. In contrast, when
475 the index is positive and high (e.g.: episodes from 1980 to 2010), we observe a 180° phase shift
476 of high coherence patterns. These findings suggest that positive and high NAO leads to a time
477 lagged impact on high altitude Alpine rivers. This is evident for the subclasses within cluster
478 NAO1, particularly after the 1980s, period when NAO starts to be significantly positive (Rossi

et al., 2011). On the other hand, streamflow time series display high coherence during considerably negative NAO. The NAO extends its influence to the Alps when the index is either significantly low or high. Mild NAO phases do not seem to have a significant impact on streamflow variability.

When the NAO index is high, alpine climate tends to respond through lower-than-average precipitation and higher-than-average temperatures (Beniston, 2006; Beniston and Jungo, 2002). This could be linked to a decrease in streamflow associated to the anti-correlated high coherence episodes at yearly scale. The opposite climate behavior is found for negative NAO phases (Casty et al., 2005). In the European Alps, relationships between the NAO and hydro-meteorological variables (e.g.: glacier surface mass balance) have proofed to be not stable over time and not always significant (Marzeion and Nesje, 2012; Vincent et al., 2017). This is because the Alps can be considered a pivotal zone between southern and northern Europe, where the correlations between the NAO index and temperature or precipitation tend to be typically strong (i.e., in the Mediterranean zone and in Scandinavia) (Beniston et al., 2018). From this analysis we can highlight that due to the Alpine region location, between the main poles of enhanced NAO–relationships (Hurrell and Van Loon, 1997; Quadrelli et al., 2001; Schmidli et al., 2002), impacts on streamflow although generally present are complex and present intermittent patterns. Thus, we can conclude that the heterogeneous catchment dynamic observed cannot be attributed to the influence of NAO only.

5.1.2.MO index

In this case, different behavior is found at the yearly scale, which leads to four clusters (MO 1- MO 4). Firstly, we identify a large cluster (MO1-1) with 64% of the stations (Table 3). At the yearly scale it presents very high, in-phase, and continuous coherence values during the

whole analyzed period. At multi-annual scales we found repeatedly a significant high-coherence pattern from 1970 to 1980 associated to the 2-4 years scale. At 4-8 years scale a pattern showing very high coherence values from around 1980 till the 1990s is detected. This pattern is prolonged in some cases with medium to high coherence values till the end of the analyzed period. We detected a particular case of two gauging stations (MOI1-2), that presented high coherence at yearly scale, but no coherence at larger scales. These two locations present a unique streamflow behavior.

At the yearly scale stations belonging to MO2 shift in the 1980s from continuous high coherence to no coherence with only sporadic high coherence spots. Stations belonging to cluster MO3 do not present continuous high coherence at yearly scale, but rather an intermittent pattern that vanishes from the 1980s. From this intermittency and no coherence patterns we can derive that MO cease its influence in the Northern region of the basin. Even a weaker yearly pattern can be recognized for MO4. In a similar manner, the yearly coherence recurs for MO2 and MO3 clusters in 2005, but the absence of coherence persists for MO4. At longer temporal scales MO2-MO4 stations behave similarly till the 1980s. In fact, significant high coherence at 4-8 years scale is present from the 1970s in all stations. The extension in time of this pattern varies however depending on the cluster. For MO2 and MO3 this pattern is prolonged till mid-1990s with less power till the present, while for MO4 this pattern is shorter and vanishes already in the early 1980s.

By applying continuous wavelet analysis, we analyzed the periodicities that characterize the MO and we observed a discontinuity from the 1980s at the yearly scale. The high-power pattern associated to the yearly scale is interrupted and Fig. 3 shows intermittent high power from the 1980s onwards. The fact that WTC shows a complete coherence at the yearly scale

means that these specific gauging stations (classified in MO1) are following a similar alteration in the periodicity. MO positive phase produces a sea level pressure anomaly field that is associated to dry periods in the central Mediterranean region, whereas the negative phase is linked to intense cyclogenesis over the central Mediterranean that produces wet conditions (Criado-Aldeanueva and Soto-Navarro, 2013). On the other hand, the stations that lose this strong coherence after the 1980s are seemingly not strongly influenced by MO (i.e., MO2, MO3 and MO4).

The annual correlations between the MO index and streamflow time series provide very high values even after the detected anomaly in the 1980s. This MO index anomaly has also been recognized as an influencing factor in neighboring regions (Martic-Bursac et al., 2017). This points out that MO variability is a valuable tool to measure atmospheric forcing in the Alps. From these insights we could conclude that MO has notable impacts on gauging stations within the Eastern Alps. However, relatively little influence is found in regions located north of the Bavarian Alps particularly from the 1980s.

5.1.3. GB index

Greenland Blocking index presents a very strong yearly periodicity, which leads to four clusters (GB1- GB4, Fig. 6c). Only GB1 presents two sub-classes (GB1-1 and GB1-2). The strong seasonality that characterizes alpine river basins is easily detectable with very high coherence values for GB1 stations, which have a mean catchment elevation above 1250 m a.s.l. (Fig. S4). Multi-temporal analysis shows diverse patterns, particularly for the cluster GB1. Stations belonging to cluster GB1 present a high coherence period between 1970 and 1980 associated to 4 years scale (although it extends in 1980 from the 2 years scale). Additional patterns emerge at the 2-4 years scale around 1990 (in-phase), 2000 (counter-phase) and 2010 (in-phase)

548 for several gauging stations classified in GB1-1. In contrast, GB1-2 stations do not present any
549 high coherence spots at multi-temporal scales after 1980. Furthermore, we capture a new
550 pattern emerging from the mid-2000s associated to the 4 years scale. These mid-2000s (2003–
551 2006) extreme high GB episodes have been related to the recent rapid loss of sea-ice to the
552 west of Greenland (starting in 1980). A delayed response (high coherence counter-phase
553 episodes) of the streamflow can be spotted during this specific period, while positive
554 coherence is found during the late 1980s and early 1990s and from 2010. These findings are
555 consistent with observed extreme negative GB events (Hanna et al., 2016). Recently, links
556 between NAO and GB have been investigated (Hanna et al., 2015; Hanna et al., 2018). GB has
557 reached a minimum during the 1980s and 1990s and therefore the eastward shift of the NAO
558 during this period has been related to the GB variability (Davini et al., 2012). This implies that
559 although the information provided by the indexes is complementary, the indexes' patterns
560 might be interlinked for specific anomalies.
561 At the yearly scale, discontinuities from the 1980s are present for several catchments located
562 within the lower Inn river basin (gauging stations belonging to GB2) with mean elevation
563 between 1000 and 1250 m a.s.l. This change in behavior is evolving from a continuous high
564 coherence at yearly scale to an intermittent presence of both high coherence and very low
565 coherence values. This finding alone highlights the evolution of the seasonality in basins with
566 the lowest mean catchment elevation and serves as indicative of the current climatic trend
567 (i.e., global warming that might affect specific river basins by changing their seasonality
568 periodicities from patterns linked to snow dominated catchments to hydrological behavior
569 associated to rain dominated basins or a combination of both).

570 **5.1.4. AO index**

571 Fig. 6d presents the spatial distribution of the clusters obtained from the WTC results between
572 streamflow time series and the Arctic Oscillation index. The AO CWT (Fig. 3d) shows that
573 AO is not characterized by a strong yearly periodicity, but it rather presents high wavelet
574 power bands at larger scales (from 2 years to 8 years scales). Thus, the clusters present several
575 subclasses, which means that several gauging stations behave similarly at the yearly scale,
576 but their coherence patterns with AO differ at longer temporal scales. We detected three
577 groups that present contrasting behaviors at yearly scale (AO1, AO2 and AO3), but additional
578 sub-classes were found for AO1 (AO1-1 to AO1-5) and AO2 (AO2-1, AO2-2) that account for
579 the larger scale variability in the coherence results.

580 At the yearly scale cluster AO1 is characterized by in phase intermittent significant high
581 coherence till 1970 and sporadic high coherence values after 1980. AO2 intermittent
582 significant high coherence is present till 1980 and it is followed by a complete loss of
583 coherence. AO3 displays similar patterns till 1980, but differs from AO2, since a counter-phase
584 significant high coherence pattern associated to the 1-2 years scale occurs in 2005.

585 When we focus on larger scales the behavior seems to have a common pattern for AO1
586 (particularly AO1-1, AO 1-3, AO1-4 and AO1-5) gauging stations till 1980. High coherence is
587 present at 4 years scale that extends from 1965 to late 1970s, followed by significant high
588 coherence at 2-4 years scales around 1980. Only AO1-2 does not present high coherence at the
589 4 years scale. Indeed, cluster AO1-2 does not show any high coherence patterns at scales larger
590 than 2 years. Besides cluster AO1-2, the remaining stations belonging to AO1 only start to
591 show different coherence patterns from the 1980s. Thus, we can distinguish different
592 behaviors after 1980 linked to larger scales. After this year at large scales AO1-1 displays two
593 main patterns: counter-phase pattern associated to 2-4 years scale till 1990 and significant high

coherence in phase around 2000. AO1-3 and AO1-4 clusters behave similarly till 2000. What characterizes AO1-3 is the reappearance of a pattern associated to 2 years scale from 2000 till 2010. In contrast, AO1-5 displays a high coherence pattern associated to the 4 years scale (in counter-phase) from the early 1980s till the 1990s. Indeed, this pattern associated to the 4 years scale seems to continue the pattern found before 1980 and is slightly migrating to even larger scales.

At larger scales, cluster AO2 presents high coherence from 1965 to late 1970s associated to the 4-6 years. Linked to 2 years scale significant coherence values in counter-phase are present only in an isolated point around 1990. For this cluster AO2 we can distinguish two different behaviors after 1980 linked to multi-annual scales. In the case of cluster AO2-1 a segment that entails from 2 to 6 years scales shows significant high coherence in counter-phase and with a 90° phase shift from 1980 till the 1990s. In contrast, AO2-2 shows significant coherence exclusively at 4 years scale with 90° phase shift. Regions of high coherence with a consistent phase relationship (e.g., 90° phase shift) imply causality between the analyzed variables (Grinsted et al., 2004; Schuler et al., 2021). Finally, AO3 does not present any coherence with AO after 1980 at 4 years scale. Different clusters show indeed a different coherence with climatic indexes from the 1980s, which highlight the increased heterogeneity of alpine rivers behavior from the 1980s. The results show that despite the correlation found between AO and NAO in past studies (Ambaum et al., 2001; Hamouda et al., 2021), different patterns are detected when analyzing multiple temporal scales.

Seven basins (Table 3) present singular behavior. These basins are representative of the smallest catchments selected for this study with catchment area not larger than 300 km^2 (minimum catchment area 100 km^2) with 70% of these basins smaller than 140 km^2. This

implies that small basins display a more complex variability that might be driven by particular geographical factors. The complexity observed in the Alps for the AO coherence with streamflow has been also found for other variables, such as snowmelt (Schaefer et al., 2004).

5.2. Classification based on all indexes and link to detected variability

The complex analysis of the coherence results points out that several gauging stations display different behaviors from the 1980s. Cold winters and significant amounts of snow, which led to high intra-annual streamflow variability, were characteristic of the Alpine region till the 1980s. From this decade, several mild winters with little snow occurred and have been linked to the presence of very persistent NAO high pressure periods (particularly in fall and winter) (Beniston and Jungo, 2002; Hurrell and Van Loon, 1997; Marty, 2008; Terzago et al., 2022). Thus, the occurrence and persistence of NAO high pressure episodes has been proved to affect the streamflow variability, decreasing it during the following years. Interestingly, with the CWT analysis we detected that for the MO the yearly pattern is also altered from then. Consequently, stations that show high coherence values with the MO during the whole analyzed time span are actually following a similar behavior at the yearly pattern. Stations located in the southern region of the Inn basin, which present higher mean elevation, are characterized by high coherence during the whole analyzed time span. In contrast, those which cease to have a strong coherence from the 1980s might not be as influenced by this climatic pattern as the abovementioned regions. This is the case for the stations located in the lower Inn basin (MO3 and MO4). We could observe therefore that the MO exhibits strong correlation with the gauging stations located in the southern region of the basin, closer to the Mediterranean Sea.

Atmospheric blocking has been associated with extreme episodes, such as cold winters and droughts and heat waves in summer, with a recent increase in frequency (Barrett et al., 2020). Thus, periods of high GB allow us to anticipate a more extreme seasonality. GB variability trends have been connected to alternating years characterized by cold winters with large snow contribution and mild winters with more unpredictable precipitation patterns (Ballinger et al., 2018; McLeod and Mote, 2015). This behavior is present in basins with mean elevation ranging from 800 to 1000 m a.s.l. (GB3).

The results presented for the AO analysis are the most complex. AO is not characterized by a strong yearly periodicity, but the multi-year scales coherence reveals interesting patterns. In fact, a similar distribution of coherence values is detected for several stations till 1980, but they start differing from this decade as has been observed with other indexes. Interestingly, the AO coherence results are the ones able to capture the particularities of some gauging stations that were considered as not classified based on streamflow dynamics. We observe that very low coherence values are found for several gauging stations. This could imply a reduced sensitivity of these gauging stations to the AO. This is particularly true for either low elevation sites in the Alps or for very high altitudes.

Negative phases of AO have been related to higher snowfall and longer persistence of winter snow cover at low-middle elevation in the Alps. On the contrary, positive phases of AO lead to unfavorable conditions for solid precipitation, since they imply dry-air advection and mild temperatures over Mediterranean regions (Terzago et al., 2022). Positive AO is present during 1979–2008 and consequently changes in the 1980s have been attributed to the interdecadal strengthening of winter AO (He et al., 2017). Similar to the NAO, Bartolini et al. (2009) stated that AO displays a rather weak correlation with winter alpine precipitation. However, it has

been proven that the influence of large scale forcing (e.g.: NAO, AO) on the Alps is not uniform in space (Terzago et al., 2022). Thus, the investigation of the correlation at multiple spatial scales becomes valuable and these results highlight that one single index does not explain entirely the observed variability.

5.3. Characterization of the clusters

We analyze the mean catchment elevation (which can be used as in this case study as a proxy for snow processes) and the glacier coverage for classes based on all indexes. Fig. 8 displays the comparison of the characteristics of each cluster by representing the mean, maximum and minimum values of glacierized area (%) and mean catchment elevation (m a.s.l.) for each class based on all indexes. Figures S3-S6 show these features for clusters based on each individual index. The mean catchment elevation seems to differentiate two groups: i) classes A-F (snow-dominated basins and mean catchment elevation higher than 1300 m a.s.l. for all stations), ii) classes G-K (rain dominated catchments with no presence of glaciers within the basins and mean catchment elevation lower than 1300 m a.s.l.). In Fig. 8b, classes B and C present the highest mean catchment elevation with mean values higher than 2250 m a.s.l.. For classes A, E and F mean values of mean catchment elevation range from 2000 to 2250 m a.s.l.. Class D however displays a lower mean catchment elevation (1900 m a.s.l.), but with a higher variability within the class (from 1330 m a.s.l. to over 2100 m a.s.l.). In contrast, within group ii) we observe that classes are also linked to a differentiated range of mean catchment elevation: for class G the range is from 1000 to 1300 m a.s.l., for class H and I from 900 to 1000 m a.s.l., for J between 800 and 900 m a.s.l., and finally for class K stations present mean catchment elevation lower than 550 m a.s.l.. These elevation intervals can be associated to the relevance of the snow processes in the basins. Additionally, the variability at yearly and multi-annual scales of singular behavior gauging stations displayed unique patterns that were

687 commonly attributed to the catchment size. The singular behavior stations are small basins
688 (<300 km^2) with an elevation range between 1500 and 2400 m a.s.l..

689 These findings could be linked to previous studies that state that above the altitudinal range
690 1500–2000 m, the snowpack is much less sensitive to the shifts in large-scale forcing. The snow
691 will likely accumulate at these altitudes on any occasion that there is precipitation, and even
692 anomalous temperatures induced by high-pressure subsidence are unlikely to be sufficient to
693 initiate melting (Beniston, 1997). In contrast, small changes in temperature or pressure could
694 indeed link to alteration in the snowpack at mid altitudes close to the melting level height.
695 The altitude where falling precipitation begins to melt has been increasing with a rapid rate
696 since the 1980s and this trend has been observed not only in the Alps but globally (Prein and
697 Heymsfield, 2020).

698 **Figure 8**

699 **5. Conclusions**

700 The present study has investigated the impact of selected oscillation indexes on streamflow
701 of representative sites of the Inn river catchment, with an additional focus on the overlap of
702 these impacts to explore streamflow variability changes detected from the 1980s. We
703 investigate the interplay of selected climate indexes and how they present heterogeneous
704 coherence patterns with the analyzed gauging stations. This study has confirmed the
705 complexity in the long-term streamflow variability of the Alps and the existence of long-term
706 cycles in streamflow behavior that are partly governed by shifts in large-scale climate indexes.
707 We observe that a shift from constant to intermittent periodicities of the MO index from the
708 1980s can be associated to changes detected in the streamflow behavior. NAO and GB extreme

709 phases are connected with cold winters and hot summers, while AO results are able to capture
710 singular hydrologic behaviors. The obtained classifications have been compared with
711 previous studies (Bartolini et al., 2009; Schaefli et al., 2007; Pérez Ciria et al., 2019; Pérez Ciria
712 and Chiogna, 2020) and we can conclude that the presented methodology gives us a quite
713 accurate representation of the heterogeneous response of streamflow in Alpine catchments.

714 The Alps can be considered a pivotal zone between southern and northern Europe and the
715 mountain range represents a transition between Mediterranean and continental domains.
716 Therefore, within a few kilometers we pass from sub-Mediterranean to glacial and
717 continental-dry climates. Moreover, several factors contribute to create different
718 microclimates, which might be more important than large scale factors. The mountainous
719 complex topography and shading effects are additional factors that have weight on the
720 catchment hydrological behavior and consequently are reflected on the streamflow time series
721 analysis. From the cluster analysis we can therefore derive how mean catchment elevation
722 and geographical location can contribute to the explanation of the influence and
723 teleconnection to the oscillation indexes, while glacierized area is not identified as a dominant
724 characteristic.

725 Following the suggested multi-temporal analysis by applying wavelet techniques, we
726 observed the existence of strong links between the temporal development of streamflow
727 variability in the Eastern Alps and specific atmospheric modes of variability. The novel
728 suggested method quantifies the similarity of climate indexes impacts on streamflow in the
729 time-frequency space. The clustering process is highly useful to better understand the
730 streamflow dynamics and to detect any recent changes in variability at specific temporal
731 scales. The approach could be applied to assess the effects and interplay of other

hydrometeorological variables. Moreover, the presented findings confirm that a fraction of the observed shifts can be attributed to decadal-scale atmospheric circulation changes. We reached a better understanding of the impacts and interplay of several climate oscillation indexes on the Eastern Alps and the resultant heterogeneity of streamflow variability. This work could be used to provide a first order prediction of the evolution of water resources in the Alpine region considering climate scenarios of atmospheric circulation and sea surface temperature conditions, along the line of recent global research in this direction (Feng et al., 2020; Ham et al., 2019; Maher et al., 2021).

Acknowledgments

The first author acknowledges funding from the Doktoratsstipendium aus der Nachwuchsförderung and Frankreich-Schwerpunkt (Reise zu französischem Kooperationspartner) from the University of Innsbruck, the TUM ForTe - Forschungsförderung und Technologietransfer and the funding from the EU Horizon 2020 innovation action programme ARSINOE (Climate-resilient regions through systemic solutions and innovations) under Grant Agreement 101037424. The author GC acknowledges the funding from the DFG (Deutsche Forschungsgemeinschaft) Research Group (FOR2793/1) "Sensitivity of High Alpine Geosystems to Climate Change since 1850" (SEHAG) (Grant CH981/3-1). The authors thank the contribution of Christopher Zier during the initial phase.

References

Agarwal A, Maheswaran R, Sehgal V, Khosa R, Sivakumar B, Bernhofer C. Hydrologic regionalization using wavelet-based multiscale entropy method. Journal of Hydrology 2016; 538: 22-32.

Ambaum MHP, Hoskins BJ, Stephenson DB. Arctic Oscillation or North Atlantic Oscillation? Journal of Climate 2001; 14: 3495-3507.

Auer I, Böhm R, Brunetti M, Maugeri M, Nanni T, Schöner W. Austrian long-term climate 1767–2000. Multiple Instrumental Climate Time Series from Central Europe (ALOCLIM). Vol 25. Vienna: Zentralanstalt für Meteorologie und Geodynamik (ZAMG), 2001.

Ballinger TJ, Hanna E, Hall RJ, Miller J, Ribergaard MH, Høyer JL. Greenland coastal air temperatures linked to Baffin Bay and Greenland Sea ice conditions during autumn through regional blocking patterns. Climate Dynamics 2018; 50: 83-100.

Barrett BS, Henderson GR, McDonnell E, Henry M, Mote T. Extreme Greenland blocking and high-latitude moisture transport. Atmospheric Science Letters 2020; 21: e1002.

Bartolini E, Claps P, D'Odorico P. Interannual variability of winter precipitation in the European Alps: relations with the North Atlantic Oscillation. Hydrology and Earth System Sciences 13 2009: 17-25.

Beniston M. Variations of snow depth and duration in the swiss alps over the last 50 years: links to changes in large-scale climatic forcings. Climatic Change 1997; 36: 49-68.

Beniston M. Mountain Weather and Climate: A General Overview and a Focus on Climatic Change in the Alps. Hydrobiologia 2006; 562: 3-16.

Beniston M, Farinotti D, Stoffel M, Andreassen LM, Coppola E, Eckert N, et al. The European mountain cryosphere: a review of its current state, trends, and future challenges. The Cryosphere 2018; 12: 759-794.

Beniston M, Jungo P. Shifts in the distributions of pressure, temperature and moisture and changes in the typical weather patterns in the Alpine region in response to the behavior of the North Atlantic Oscillation. Theoretical and Applied Climatology 2002; 71: 29-42.

Blöschl G, Hall J, Viglione A, Perdigão RAP, Parajka J, Merz B, et al. Changing climate both increases and decreases European river floods. Nature 2019; 573: 108-111.

Bocchiola D. Long term (1921–2011) hydrological regime of Alpine catchments in Northern Italy. Advances in Water Resources 2014; 70: 51–64.

Box JE, Decker DT. Greenland marine-terminating glacier area changes: 2000–2010. Annals of Glaciology 2011; 52: 91-98.

Brunetti M, Maugeri M, Nanni T. Atmospheric circulation and precipitation in Italy for the last 50 years. International Journal of Climatology 2002; 22: 1455-1471.

Buckel J, Otto J-C. The Austrian Glacier Inventory GI 4 (2015) in ArcGis (shapefile) format. PANGAEA, 2018.

Casty C, Wanner H, Luterbacher J, Esper J, Böhm R. Temperature and precipitation variability in the European Alps since 1500. International Journal of Climatology 2005; 25: 1855-1880.

Cenk S, Turgay P. The effects of Mediterranean oscillation on temperature and precipitation data in Turkey. Journal of Water and Climate Change 2019; 11: 722-743.

Conte M, Giuffrida A, Tedesco S. The Mediterranean Oscillation. Impact on precipitation and hydrology in Italy Climate Water. Publications of the Academy of Finland, Helsinki 1989.

Corella J, Valero-Garcés B, Vicente-Serrano S, Brauer A, Benito G. Three millennia of heavy rainfalls in Western Mediterranean: Frequency, seasonality and atmospheric drivers. Scientific Reports 2016; 6: 38206.

Criado-Aldeanueva F, Soto-Navarro J. The Mediterranean Oscillation Teleconnection Index: Station-Based versus Principal Component Paradigms. Advances in Meteorology 2013; 2013: 1-10.

Dahlman L. Climate Variability: North Atlantic Oscillation. National Oceanic and Atmospheric Administration (NOAA), 2009.

Das J, Jha S, Goyal MK. On the relationship of climatic and monsoon teleconnections with monthly precipitation over meteorologically homogenous regions in India: Wavelet & global coherence approaches. Atmospheric Research 2020; 238: 104889.

Davini P, Cagnazzo C, Neale R, Tribbia J. Coupling between Greenland blocking and the North Atlantic Oscillation pattern. Geophysical Research Letters 2012; 39.

Dünkeloh A, Jacobeit J. Circulation dynamics of Mediterranean precipitation variability 1948–98. International Journal of Climatology 2003; 23: 1843-1866.

807 Efthymiadis D, Jones PD, Briffa KR, Böhm R, Maugeri M. Influence of large-scale atmospheric
808 circulation on climate variability in the Greater Alpine Region of Europe. Journal of
809 Geophysical Research: Atmospheres 2007; 112.
810 Engel M, Penna D, Bertoldi G, Vignoli G, Tirler W, Comiti F. Controls on spatial and temporal variability
811 in streamflow and hydrochemistry in a glacierized catchment. Hydrol. Earth Syst. Sci. 2019;
812 23: 2041-2063.
813 Feidas H, Noulopoulou C, Makrogiannis T, Bora-Senta E. Trend analysis of precipitation time series in
814 Greece and their relationship with circulation using surface and satellite data: 1955–2001.
815 Theoretical and Applied Climatology 2007; 87: 155-177.
816 P. Feng, B. Wang, J.-J. Luo, D.L. Liu, C. Waters, F. Ji, H. Ruan, D. Xiao, L. Shi, Q. Yu
817 Using large-scale climate drivers to forecast meteorological drought condition in growing season
818 across the Australian wheatbelt. Sci. The Total Environ. 2020; 724.
819 Fraedrich K. An ENSO impact on Europe? Tellus A 1994; 46: 541-552.
820 Fu C, James AL, Wachowiak MP. Analyzing the combined influence of solar activity and El Niño on
821 streamflow across southern Canada. Water Resources Research 2012; 48.
822 Gong D-Y, Wang S-W, Zhu J-H. East Asian Winter Monsoon and Arctic Oscillation. Geophysical
823 Research Letters 2001; 28: 2073-2076.
824 Gong D, Wang S. Definition of Antarctic Oscillation index. Geophysical Research Letters 1999; 26: 459-
825 462.
826 Grinsted A, Moore JC, Jevrejeva S. Application of the cross wavelet transform and wavelet coherence
827 to geophysical time series. Nonlinear processes in geophysics 2004; 11: 561-566.
828 Ham, YG., Kim, JH. & Luo, JJ. Deep learning for multi-year ENSO forecasts. Nature 2019; 573, 568–572.
829 https://doi.org/10.1038/s41586-019-1559-7
830 Hamouda M, Pasquero C, Tziperman E. Decoupling of the Arctic Oscillation and North Atlantic
831 Oscillation in a warmer climate. Nature Climate Change 2021; 11.
832 Hanna E, Cropper TE, Hall RJ, Cappelen J. Greenland Blocking Index 1851–2015: a regional climate
833 change signal. International Journal of Climatology 2016; 36: 4847-4861.
834 Hanna E, Cropper TE, Jones PD, Scaife AA, Allan R. Recent seasonal asymmetric changes in the NAO (a
835 marked summer decline and increased winter variability) and associated changes in the AO
836 and Greenland Blocking Index. International Journal of Climatology 2015; 35: 2540-2554.
837 Hanna E, Hall RJ, Cropper TE, Ballinger TJ, Wake L, Mote T, et al. Greenland blocking index daily series
838 1851–2015: Analysis of changes in extremes and links with North Atlantic and UK climate
839 variability and change. International Journal of Climatology 2018; 38: 3546-3564.
840 He Q, Chun KP, Tan ML, Dieppois B, Juneng L, Klaus J, et al. Tropical drought patterns and their linkages
841 to large-scale climate variability over Peninsular Malaysia. Hydrological Processes 2021; 35:
842 e14356.
843 He S, Gao Y, Li F, Wang H, He Y. Impact of Arctic Oscillation on the East Asian climate: A review. Earth-
844 Science Reviews 2017; 164: 48-62.
845 Hurrell JW, Van Loon H. DECADAL VARIATIONS IN CLIMATE ASSOCIATED WITH THE NORTH ATLANTIC
846 OSCILLATION. Climatic Change 1997; 36: 301-326.
847 Jevrejeva S, Moore JC, Grinsted A. Influence of the Arctic Oscillation and El Niño-Southern Oscillation
848 (ENSO) on ice conditions in the Baltic Sea: The wavelet approach. Journal of Geophysical
849 Research: Atmospheres 2003; 108.
850 Kahya E, Kalaycı S. Trend analysis of streamflow in Turkey. Journal of Hydrology 2004; 289: 128-144.
851 Kerr RA. A New Force in High-Latitude Climate. Science 1999; 284: 241-242.
852 Korck J, Danneberg J, Willems W. Impacts of climate change on the water regime of the Inn River basin
853 - extracting adaptation-relevant information from climate model ensembles and impact
854 modelling. Advances in Geosciences 2012; 32: 99-107.
855 Labat D. Wavelet analysis of the annual discharge records of the world's largest rivers. Advances in
856 Water Resources 31 2008: 109-117.

Labat D. Cross wavelet analyses of annual continental freshwater discharge and selected climate indices. Journal of Hydrology 2010; 385: 269-278.
Labat D, Ronchail J, Callede J, Guyot JL, De Oliveira E, Guimaraes W. Wavelet analysis of Amazon hydrological regime variability. Geophysical Research Letters 2004; 31.
Lehr C, Ward PJ, Kummu M. Impact of Large-scale Climatic Oscillations on Snowfall-related Climate Parameters in the World's Major Downhill Ski Areas: A Review. Mountain Research and Development 2012; 32: 431-445, 15.
Ley R, Casper MC, Hellebrand H, Merz R. Catchment classification by runoff behaviour with self-organizing maps (SOM). Hydrol. Earth Syst. Sci. 2011; 15: 2947-2962.
Linsbauer A, Huss M, Hodel E, Bauder A, Fischer M, Weidmann Y, et al. The New Swiss Glacier Inventory SGI2016: From a Topographical to a Glaciological Dataset. Frontiers in Earth Science 2021; 9.
Maher, N., Power, S.B. & Marotzke, J. More accurate quantification of model-to-model agreement in externally forced climatic responses over the coming century. Nature Communications 2021; 12, 788. https://doi.org/10.1038/s41467-020-20635-w
Malagó A, Bouraoui F, Vigiak O, Grizzetti B, Pastori M. Modelling water and nutrient fluxes in the Danube River Basin with SWAT. Science of The Total Environment 2017; 603-604: 196-218.
Maraun D, Kurths J. Cross wavelet analysis: significance testing and pitfalls. Nonlinear Processes in Geophysics 2004; 11: 505-514.
Marcolini G, Bellin A, Disse M, Chiogna G. Variability in snow depth time series in the Adige catchment. Journal of Hydrology: Regional Studies 2017; 13: 240-254.
Martic-Bursac N, Bursać BL, Ducić VD, Radivojevic A, Nenad Ž, Ivanovic R, et al. The impact of mediterranean oscillations on periodicity and trend of temperature in the valley of the Nisava River - A Fourier and wavelet approach. Thermal Science 2017; 21: 1389-1398.
Marty C. Regime shift of snow days in Switzerland. Geophysical Research Letters 2008; 35.
Marzeion B, Nesje A. Spatial patterns of North Atlantic Oscillation influence on mass balance variability of European glaciers. The Cryosphere 2012; 6: 661-673.
Massei N, Laignel B, Deloffre J, Mesquita J, Motelay A, Lafite R, et al. Long-term hydrological changes of the Seine River flow (France) and their relation to the North Atlantic Oscillation over the period 1950–2008. International Journal of Climatology 2010; 30: 2146-2154.
Massei N, Laignel B, Rosero E, Motelay-massei A, Deloffre J, Yang Z-L, et al. A wavelet approach to the short-term to pluri-decennal variability of streamflow in the Mississippi river basin from 1934 to 1998. International Journal of Climatology 2011; 31: 31-43.
Matiu M, Crespi A, Bertoldi G, Carmagnola CM, Marty C, Morin S, et al. Observed snow depth trends in the European Alps: 1971 to 2019. The Cryosphere 2021; 15: 1343-1382.
McLeod JT, Mote TL. Assessing the role of precursor cyclones on the formation of extreme Greenland blocking episodes and their impact on summer melting across the Greenland ice sheet. Journal of Geophysical Research: Atmospheres 2015; 120: 12357-12377.
Michel C, Madonna E, Spensberger C, Li C, Outten S. Dynamical drivers of Greenland blocking in climate models. Weather Clim. Dynam. 2021; 2: 1131-1148.
Nalley D, Adamowski J, Khalil B. Using discrete wavelet transforms to analyze trends in streamflow and precipitation in Quebec and Ontario (1954–2008). Journal of Hydrology 2012; 475: 204-228.
Nalley D, Adamowski J, Khalil B, Biswas A. Inter-annual to inter-decadal streamflow variability in Quebec and Ontario in relation to dominant large-scale climate indices. Journal of Hydrology 2016; 536: 426-446.
Nalley D, Adamowski J, Biswas A, Gharabaghi B, Hu W. A multiscale and multivariate analysis of precipitation and streamflow variability in relation to ENSO, NAO and PDO. Journal of Hydrology 2019; 574: 288-307.

Ntegeka V, Salamon P, Gomes G, Sint H, Lorini V, Zambrano-Bigiarini M, et al. EFAS-Meteo: A European daily high-resolution gridded meteorological data set for 1990 - 2011. In: Commission JRCotE, editor, 2013.
Palutikof JP. Analysis of Mediterranean climate data: measured and modelled. In: Bolle HJ, editor. Mediterranean climate: Variability and trends. Springer-Verlag, Berlin, 2003.
Palutikof JP, Conte M, Casimiro Mendes J, Goodess CD, Espirito Santo F. Climate and climatic change. In: Brandt CJ, Thornes JB, editors. Mediterranean Desertification and Land Use. John Wiley & Sons, London, 1996, pp. 43–86.
Partal T. Wavelet transformвЂђbased analysis of periodicities and trends of Sakarya basin (Turkey) streamflow data. River Research and Applications 2010; 26: 711.
Pasquini AI, Depetris PJ. Discharge trends and flow dynamics of South American rivers draining the southern Atlantic seaboard: An overview. Journal of Hydrology 2007; 333: 385-399.
Pelly JL, Hoskins BJ. A New Perspective on Blocking. Journal of the Atmospheric Sciences 2003; 60: 743-755.
Pérez Ciria T, Chiogna G. Intra-catchment comparison and classification of long-term streamflow variability in the Alps using wavelet analysis. Journal of Hydrology 2020; 587: 124927.
Pérez Ciria T, Labat D, Chiogna G. Detection and interpretation of recent and historical streamflow alterations caused by river damming and hydropower production in the Adige and Inn river basins using continuous, discrete and multiresolution wavelet analysis. Journal of Hydrology 2019; 578: 124021.
Prein A, Heymsfield A. Increased melting level height impacts surface precipitation phase and intensity. Nature Climate Change 2020; 10: 1-6.
Quadrelli R, Lazzeri M, Cacciamani C, Tibaldi S. Observed winter Alpine precipitation variability and links with large-scale circulation patterns. Climate Research 2001; 17: 275-284.
Ranzi R, Michailidi EM, Tomirotti M, Crespi A, Brunetti M, Maugeri M. A multi-century meteo-hydrological analysis for the Adda river basin (Central Alps). Part II: Daily runoff (1845–2016) at different scales. International Journal of Climatology 2021; 41: 181-199.
Redolat D, Monjo R, Lopez-Bustins JA, Martin-Vide J. Upper-Level Mediterranean Oscillation index and seasonal variability of rainfall and temperature. Theoretical and Applied Climatology 2019; 135: 1059-1077.
Rossi A, Massei N, Laignel B. A synthesis of the time-scale variability of commonly used climate indices using continuous wavelet transform. Global and Planetary Change 2011; 78: 1-13.
Rossi A, Massei N, Laignel B, Sebag D, Copard Y. The response of the Mississippi River to climate fluctuations and reservoir construction as indicated by wavelet analysis of streamflow and suspended-sediment load, 1950–1975. Journal of Hydrology 2009; 377: 237-244.
Rottler E, Francke T, Bürger G, Bronstert A. Long-term changes in central European river discharge for 1869–2016: impact of changing snow covers, reservoir constructions and an intensified hydrological cycle. Hydrol. Earth Syst. Sci. 2020; 24: 1721-1740.
Sang YF, Sun F, Singh VP, Xie P, Sun J. A discrete wavelet spectrum approach for identifying non-monotonic trends in hydroclimate data. Hydrol. Earth Syst. Sci. 2018; 22: 757-766.
Schaefer K, Denning AS, Leonard O. The winter Arctic Oscillation and the timing of snowmelt in Europe. Geophysical Research Letters 2004; 31.
Schaefli B, Maraun D, Holschneider M. What drives high flow events in the Swiss Alps? Recent developments in wavelet spectral analysis and their application to hydrology. Advances in Water Resources 2007; 30: 2511-2525.
Schäffer R, Sass I, Heldmann C-D, Hesse JC, Hintze M, Scheuvens D, et al. Wasserwirtschaftliche Schlussfolgerungen aus der Stichtagsbeprobung eines 225 km2 großen Einzugsgebietes im NW Tauernfenster, Österreich. Grundwasser 2020; 25: 53-68.
Scherrer SC, Appenzeller C, Laternser M. Trends in Swiss Alpine snow days: The role of local- and large-scale climate variability. Geophysical Research Letters 2004; 31.

957 Schmidli J, Schmutz C, Frei C, Wanner H, Schär C. Mesoscale precipitation variability in the region of
958 the European Alps during the 20th century. International Journal of Climatology 2002; 22:
959 1049–1074.
960 Schuler P, Cantoni È, Duran L, Johnston P, Gill L. Using Wavelet Coherence to Characterize Surface
961 Water Infiltration into a Low-Lying Karst Aquifer. Groundwater 2021; 59: 71-79.
962 Soja G, Züger J, Knoflacher M, Kinner P, Soja A-M. Climate impacts on water balance of a shallow
963 steppe lake in Eastern Austria (Lake Neusiedl). Journal of Hydrology 2013; 480: 115-124.
964 Stahl K, Moore RD, Shea JM, Hutchinson D, Cannon AJ. Coupled modelling of glacier and streamflow
965 response to future climate scenarios. Water Resources Research 2008; 44.
966 Steirou E, Gerlitz L, Apel H, Merz B. Links between large-scale circulation patterns and streamflow in
967 Central Europe: A review. Journal of Hydrology 2017; 549: 484-500.
968 Stewart IT. Changes in snowpack and snowmelt runoff for key mountain regions. Hydrological
969 Processes 2009; 23: 78-94.
970 Terzago S, Fratianni S, Cremonini R. Italian Alps (1926-2010): trends and connections with the North
971 Atlantic/Arctic Oscillation. METEOROLOGY AND ATMOSPHERIC PHYSICS. 704 pp: 125-136.
972 2022.
973 Thompson DWJ, Wallace JM. The Arctic oscillation signature in the wintertime geopotential height
974 and temperature fields. Geophysical Research Letters 1998; 25: 1297-1300.
975 Thompson DWJ, Wallace JM. Annular Modes in the Extratropical Circulation. Part I: Month-to-Month
976 Variability. Journal of Climate 2000; 13: 1000-1016.
977 Törnros T. On the relationship between the Mediterranean Oscillation and winter precipitation in the
978 Southern Levant. Atmospheric Science Letters 2013; 14: 287-293.
979 Torrence C, Compo GP. A practical guide to wavelet analysis. Bulletin of the American Meteorological
980 society 1998; 79: 61-78.
981 Torrence C, Webster PJ. Interdecadal Changes in the ENSO–Monsoon System. JOURNAL OF CLIMATE
982 1999; 12: 2679-2690.
983 Tsimplis MN, Shaw AGP. The forcing of mean sea level variability around Europe. Global and Planetary
984 Change 2008; 63: 196-202.
985 van den Broeke MR, Enderlin EM, Howat IM, Kuipers Munneke P, Noël BPY, van de Berg WJ, et al. On
986 the recent contribution of the Greenland ice sheet to sea level change. The Cryosphere 2016;
987 10: 1933-1946.
988 Vincent C, Fischer A, Mayer C, Bauder A, Galos SP, Funk M, et al. Common climatic signal from glaciers
989 in the European Alps over the last 50 years. Geophysical Research Letters 2017; 44: 1376-
990 1383.
991 Wanders N, Wada Y. Decadal predictability of river discharge with climate oscillations over the 20th
992 and early 21st century. America Geophysical Union Publications 2015: 1-7.
993 Woollings T, Barriopedro D, Methven J, Son S-W, Martius O, Harvey B, et al. Blocking and its Response
994 to Climate Change. Current Climate Change Reports 2018; 4: 287-300.
995 Yeditha PK, Rathinasamy M, Agarwal A, Sivakumar B. Intercomparison of downscaling methods for
996 daily precipitation with emphasis on wavelet-based hybrid models. Journal of Hydrology 2021;
997 599: 126373.
998 Zolezzi G, Bellin A, Bruno MC, Maiolini B, Siviglia A. Assessing hydrological alterations at multiple
999 temporal scales: Adige River, Italy. Water Resources Research 2009; 45.

1000

Figure captions

Fig. 1. a) Overview of the study domain showing the elevation and location of the selected streamflow gauging stations along the Inn River and its tributaries (identified by gauging station IDs described in Table 1); b) Inn river basin with the classification of the gauging stations based on streamflow dynamics after Pérez Ciria and Chiogna (2020). Plot b shows the classes considering the different streamflow behaviors detected at multiple temporal scales. Each cluster represents stations with correlation coefficient higher than 0.85 for all analyzed temporal scales.

Fig. 2. Methodological flowchart of the wavelet analysis, clustering process to obtain the classification based on each individual index, based on all indexes and comparison with catchment classification based on streamflow dynamics of the Inn River basin.

Fig. 3. Continuous Wavelet Transform (CWT) of a) NAO, b) MO, c) GB, and d) AO indexes time series. The x axis displays the analyzed time span (years) and the y axis the different investigated periods (temporal scales). The shadowed area indicates regions inside the COI, where edge effects can occur. Colors range from red (high wavelet power associated to periodicities in the signal) to blue (low wavelet power). The black contour lines indicate 95% confidence level.

Fig. 4. Wavelet Transform Coherence among considered climate indexes (NAO, MO, GB, and AO). The focus is on long temporal scales (i.e. yearly, 2–8 years scales). The x axis displays the analyzed time span (years) and the y axis the different investigated periods (temporal scales). The color of the plot ranges from blue, which means no coherence between the variables (value equal to 0), to red, which means total coherence (value equal to 1). The black contour lines indicate 95% confidence level. The relative phase relationship between variables is represented by arrows: arrows pointing right represent in-phase coherence and pointing left a counter-phase behavior.

Fig. 5. WTC between climatic indexes (NAO, MO, AO, and GB) and three different gauging stations representing different coherence results. Plots a-d) show the results of the WTC with the gauging station Innsbruck (ID 16), plots e-h) show the gauging station Kirchbichl (ID 20). These two gauging stations present very similar coherence patterns with the four climatic indexes and belong therefore to the same class. In contrast, plots i-l) show the gauging station Anger (ID 1), which belongs to a different class. The x axis displays the analyzed time span (years) and the y axis the different investigated periods (temporal scales). The focus is on long temporal scales (i.e. yearly, 2–8 years scales). The color of the plot and the arrows description is analogous to Fig. 4.

Fig. 6. Geographical distribution of the different classes obtained from the WTC analysis of 50 gauging stations along the Inn River and its tributaries with climate oscillation indexes: a) , b) MO, c) GB, and d) AO indexes. The maps show the heterogeneous response of gauging stations, which are clustered based on the observed patterns at i) the yearly scale (represented by the first number that follows the climate index acronym), and ii) longer scales (only represented by a second number indicating a sub-class for gauging station that even showing the same yearly patterns display a different behavior when analyzing longer temporal scales). Gauging stations that display a similar behavior at the yearly scale share the same symbol color (e.g.: green for NAO1). Sub-classes derived from groups of gauging station with the same patterns at yearly scale, but different behavior at longer temporal scales are represented with different symbols (e.g.: cross for NAO1-1 and triangle for NAO1-2). In addition, gauging stations categorized as having singular behavior are represented with a grey cross.

Fig. 7. Overlay of clusters showing the heterogeneous response of gauging stations of the Inn catchment to climatic indices. Plot a) presents the classification based on all indexes (classes A-K) and gauging stations with singular behavior (i.e., basins which were not classified for a specific index). The detailed explanation of the definition of each class is presented in Table 3. Plot b) displays the level of agreement (described in detail in section 3.3) between the classification based on all indexes showed in plot a) and the classification based on streamflow dynamics presented in Pérez Ciria and Chiogna (2020) (Fig. 1b).

Fig. 8. Comparison of the characteristics of each cluster by representing the mean (symbolized with a circle), maximum and minimum values (symbolized with "+") of glacierized area (%) and mean catchment elevation (m a.s.l.) for each group of gauging stations that belong to the same class for the conducted analysis with the different climate oscillation indexes (classification based on all indexes in Table 3). Please note that classes F, H and J only have one gauging station and therefore only one value is shown (symbolized with a circle as the mean for other classes). The number of gauging stations attributed to each class is shown in Table 4.

Figure1

Click here to access/download;Figure;Figure1_final.jpg

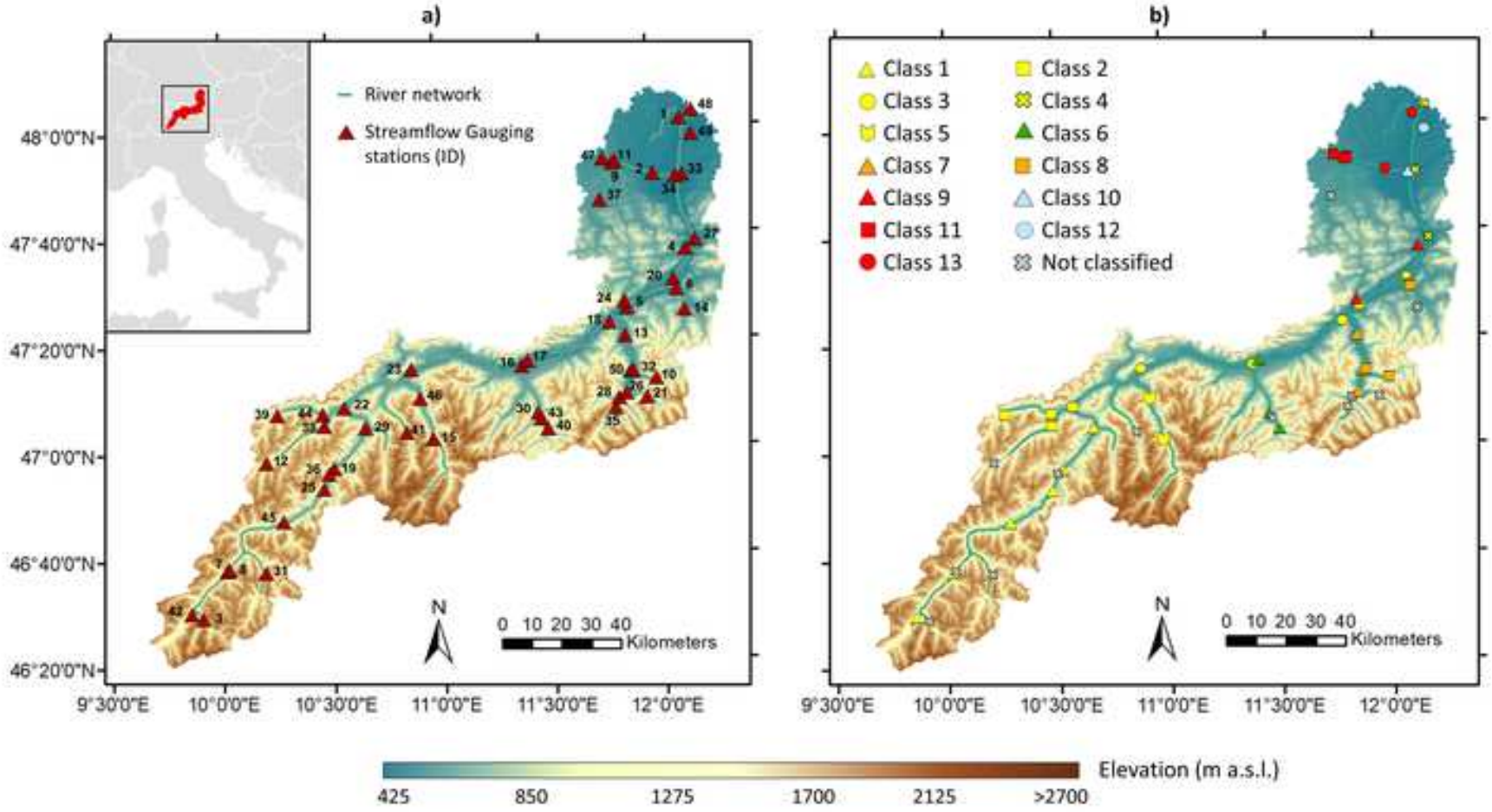

Figure2

Click here to access/download;Figure;Figure2_updated.jpg

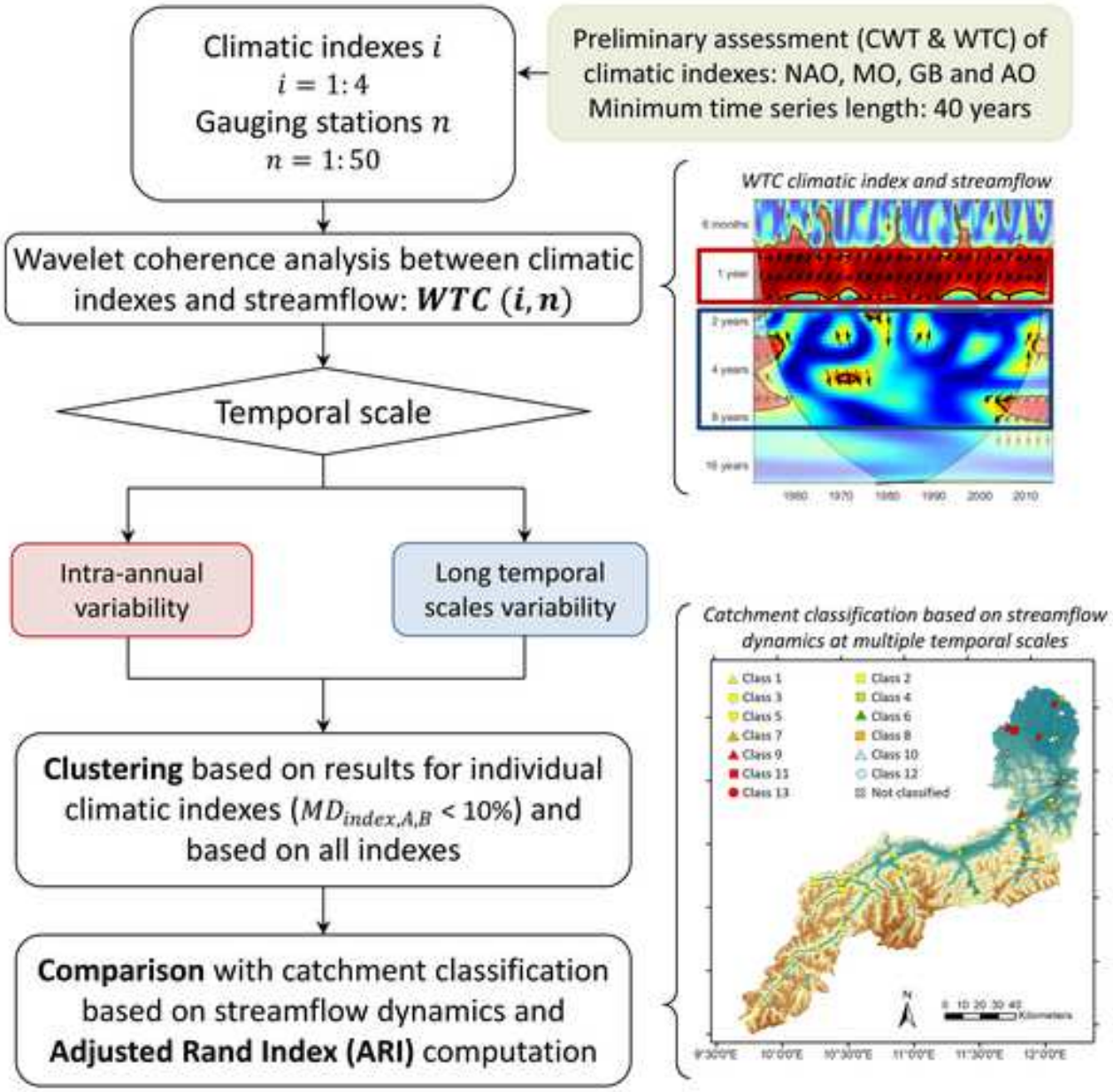

Figure3

Click here to access/download;Figure;Figure3.jpg

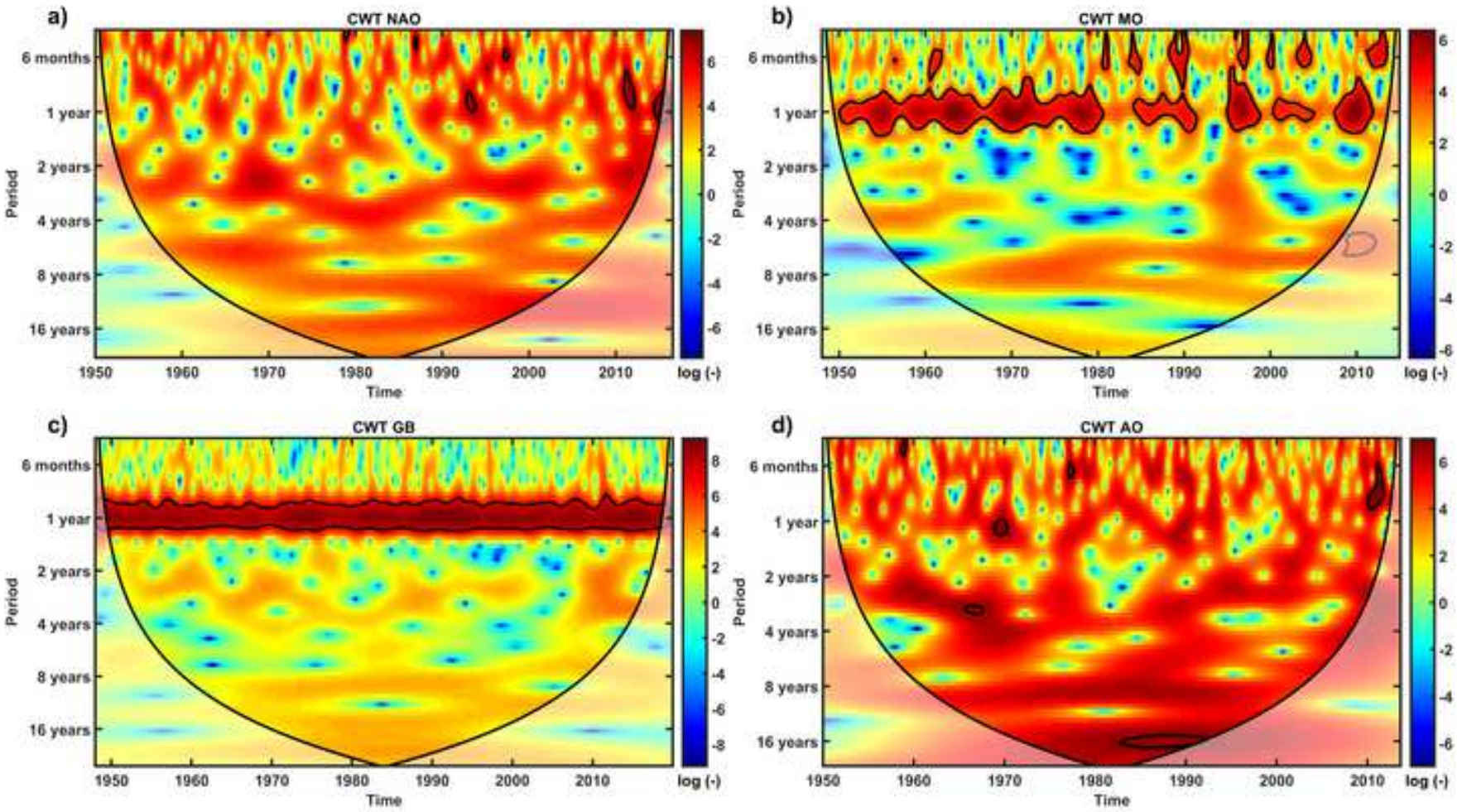

Figure4

Click here to access/download;Figure;Figure4.jpg

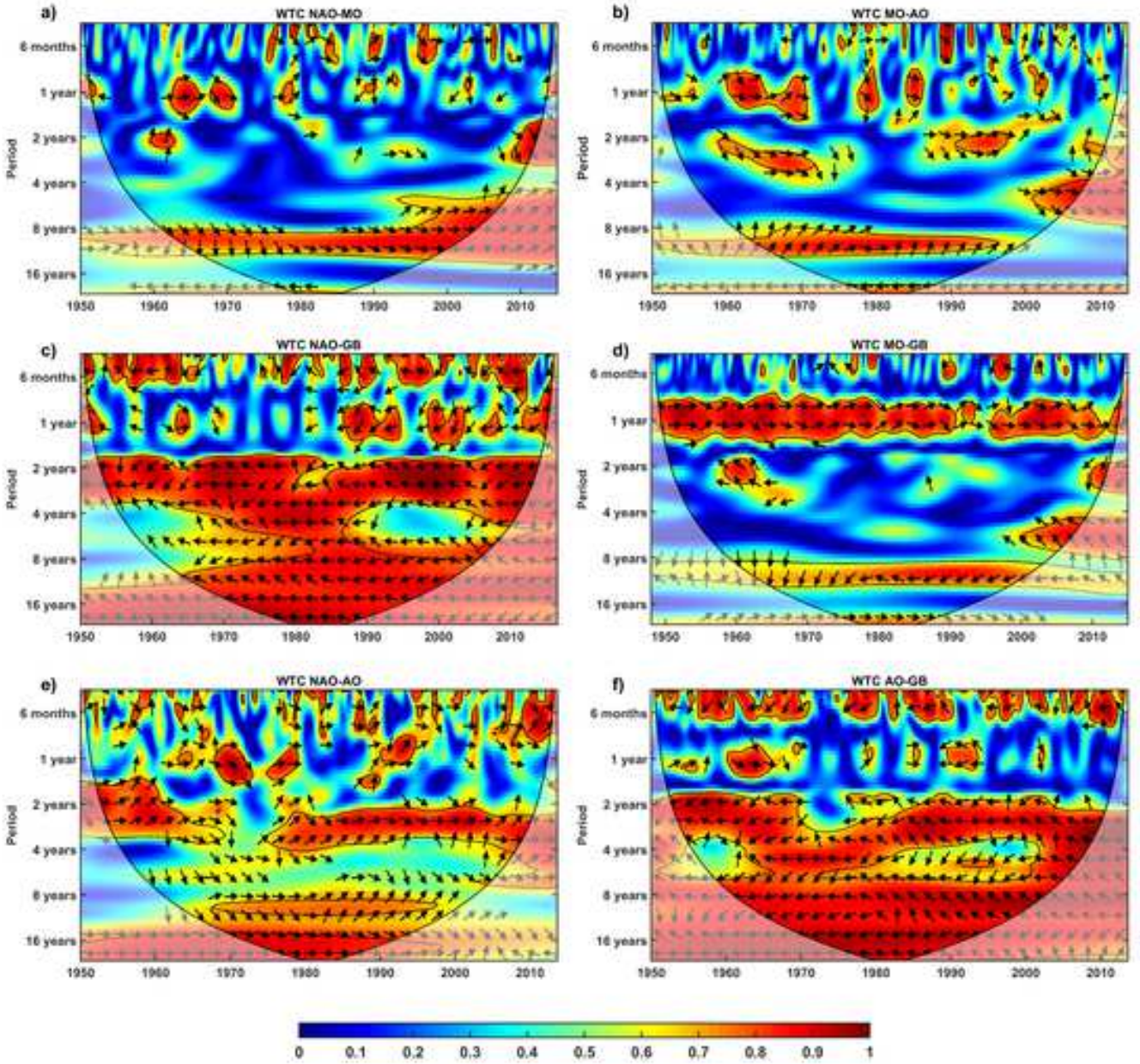

Figure5

Click here to access/download;Figure;Figure5.jpg

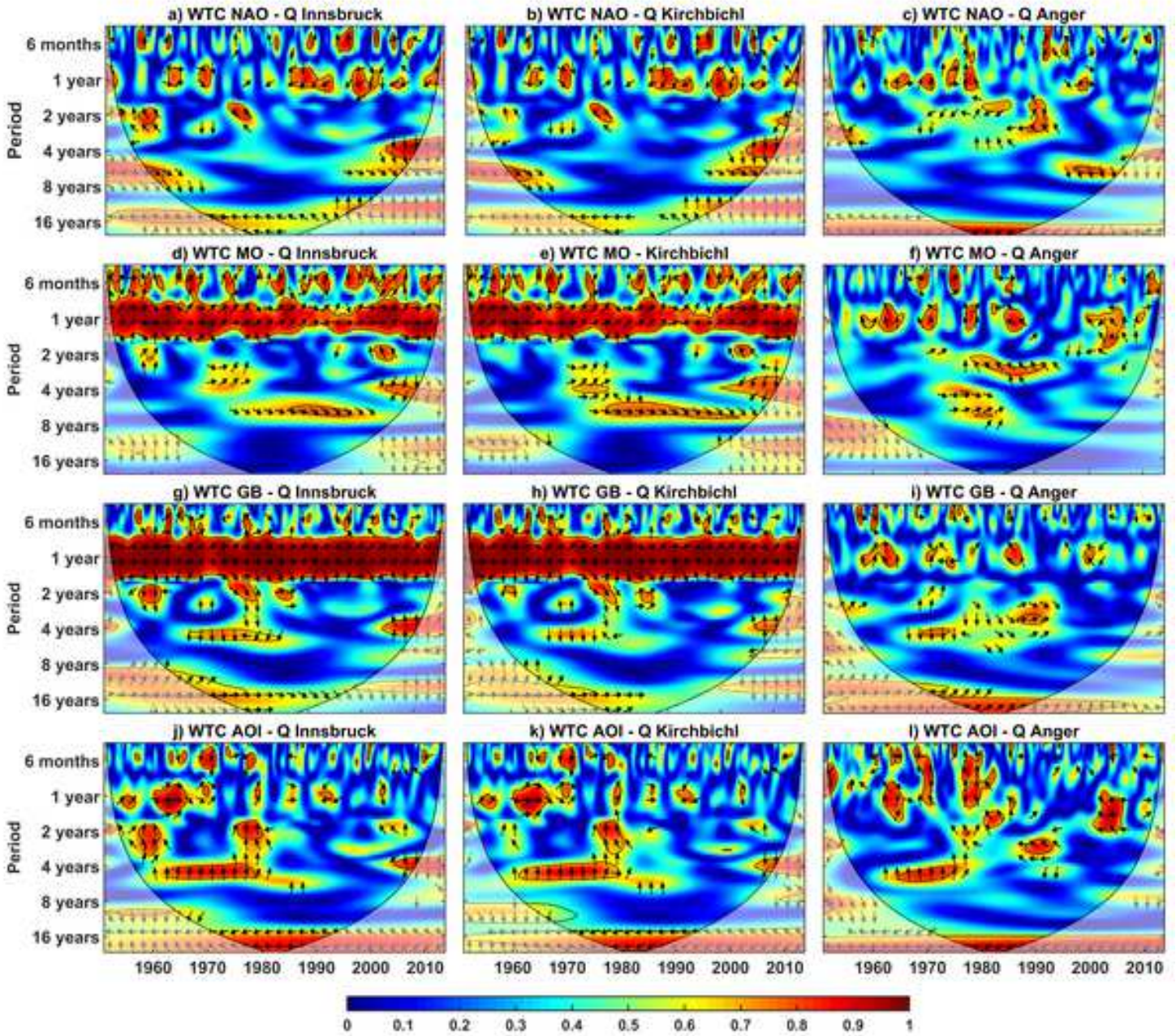

Figure6

Click here to access/download;Figure;Figure6.jpg

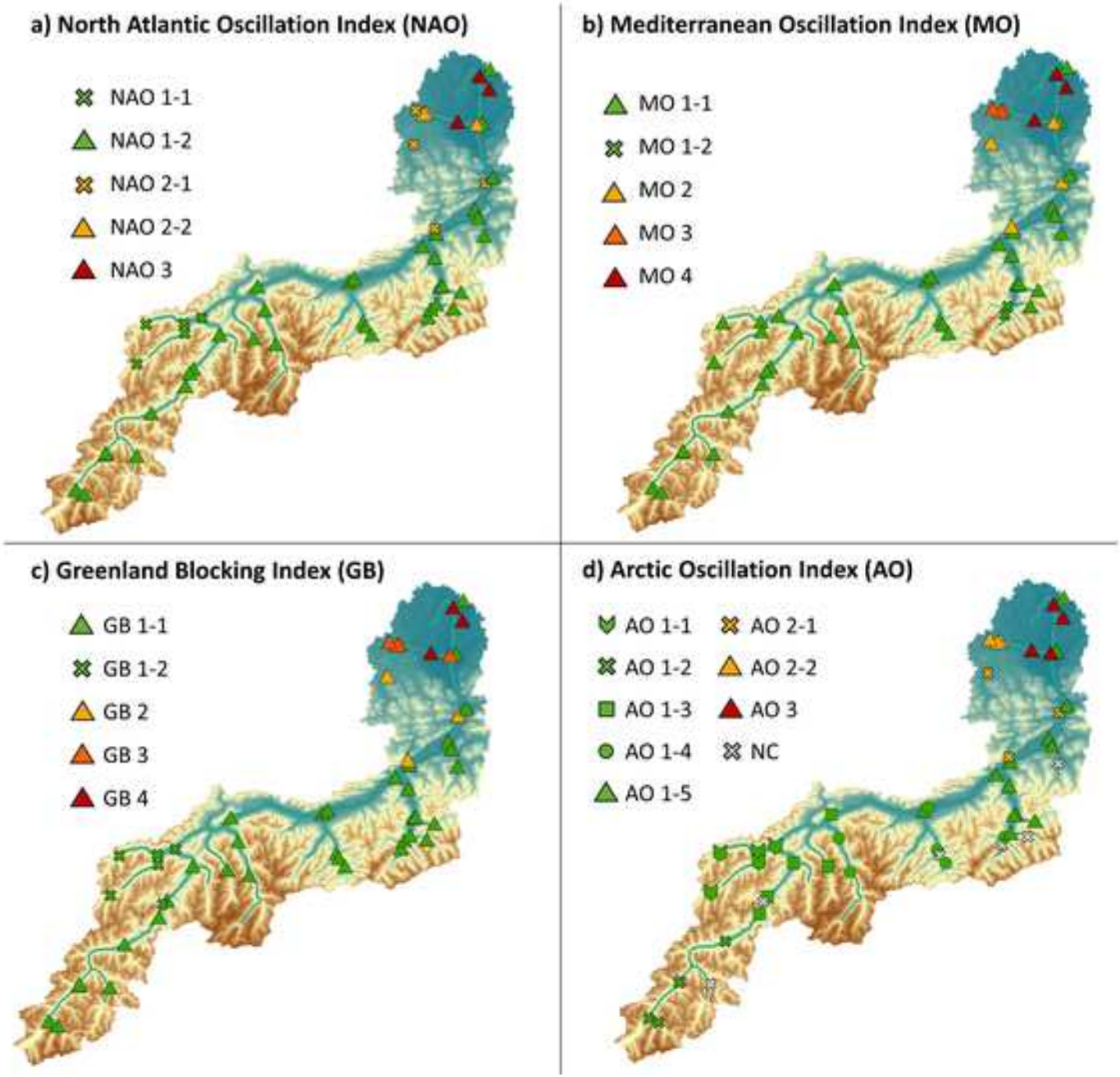

Figure7

Click here to access/download;Figure;figure 7_updated.jpg